RESEARCH ARTICLE

Zasp52's differentially expressed intrinsically disordered region confers thin filament stability at the Z-disc

Nikolai Ho, Frieder Schöck*

Department of Biology, McGill University, Montreal, Canada

eLife Assessment

This study investigates the role of the Z-disc protein Zasp52 in Drosophila flight muscles and provides evidence that an intrinsically disordered region (IDR) helps to stabilize and promote the localization of the protein to the Z-disc. Overall, this represents an **important** study that provides insights into Z-disc function and maintenance. The data are **convincing**, supported by strong genetic evidence and behavioral tests, well-controlled experiments, and detailed statistical analyses. Characterization of a new actin-binding motif mutant and FRAP analysis further support the functional importance of the Zasp52 IDR.

***For correspondence:** frieder.schoeck@mcgill.ca

Competing interest: The authors declare that no competing interests exist.

Funding: See page 20

Preprint posted
15 March 2026
Sent for Review
09 March 2026
Reviewed preprint v1
14 May 2026
Reviewed preprint v2
18 August 2026
Version of Record
27 August 2026

Reviewing Editor: Michael Buszczak, University of Texas Southwestern Medical Center, United States

© Copyright Ho and Schöck. This article is distributed under the terms of the Creative Commons Attribution License, which permits unrestricted use and redistribution provided that the original author and source are credited.

Abstract The *Drosophila* scaffolding protein Zasp52 is required to maintain structure at the muscle Z-disc, which experiences strong forces during contraction. It is alternatively spliced into many isoforms, some of which contain a long intrinsically disordered region (IDR). We show that this region is primarily expressed in the indirect flight muscle (IFM) and is required for maintaining the integrity of the Z-disc. Deleting the IDR-encoding exon 15e results in flightlessness and structural IFM defects, including sarcomere bending at the Z-disc and an inability to de-contract. These defects are indicative of a lack of proper thin filament anchoring to the Z-disc. This is further supported by a genetic interaction between exon 15e and actin. Fluorescence recovery after photobleaching of an isoform lacking exon 15e shows that the IDR is required for maintaining Zasp52 at the Z-disc and thereby stabilizing Z-discs. Lastly, we can rescue these phenotypes by restricting IFM use. Together, these results suggest that Zasp52's IDR confers thin filament stability at the Z-disc of IFM.

Introduction

The fruit fly *Drosophila melanogaster* possesses 152 muscle groups in the imago, as well as 54 in the larva (***Bothe and Baylies, 2016***). Each muscle is adapted to perform a specialized function, such as the extremely ordered indirect flight muscle (IFM), which is designed to enable the rapid oscillatory contractions needed to sustain flight. The marked phenotypic differences among these muscle types beg a molecular explanation. Alternative splicing is known to contribute to muscle-type development and function, with about 80% of sarcomere proteins being differentially expressed or spliced in *Drosophila* muscle (***Nikonova et al., 2020***). One such protein is Zasp52, a scaffolder, which contains numerous alternatively spliced exons generating a variety of isoforms.

All metazoan muscles share considerable structural homology (***Steinmetz et al., 2012***). They come in two types: striated, which appear striped given the presence of sarcomeres, and smooth, which do not possess sarcomeres. The sarcomere, a cylindrical structure, is the fundamental contractile unit of striated muscle and is bordered on either side by a dense circular structure called the Z-disc.

Sarcomeres are arranged end-to-end in long arrays called myofibrils. Thin filaments composed of actin are anchored at and extend perpendicularly from the Z-disc into neighboring sarcomeres, terminating at the H-zone (the region halfway between two Z-discs with no thin filaments). Thick filaments composed of muscle myosin are centered at the M-line (found at the center of the H-zone) and interdigitate with thin filaments in a hexagonal lattice. The mechanism of sarcomere contraction is explained by the sliding filament theory in which thick filaments pull upon thin filaments in an ATP-dependent manner, bringing the Z-discs closer together. The simultaneous contraction of tandem sarcomeres comprising a myofibril is what leads to large-scale muscular contraction (***Krans, 2010***). The Z-disc is crucial for maintaining mechanical stability of the muscle and contains numerous proteins, including Zasp52, which interacts with the thin filament cross-linker α-actinin (***Liao et al., 2016***) and actin (***Liao et al., 2020***) in *Drosophila*.

Zasp52, part of the three-membered *Drosophila* Alp/Enigma protein family along with Zasp66 and Zasp67, is crucial for maintaining structure at the Z-disc. It localizes to the Z-disc in all muscle types of *D. melanogaster* (***Katzemich et al., 2011***) and is required for the assembly and maintenance of IFM sarcomeres (***Katzemich et al., 2013***; ***Liao et al., 2016***; ***Medina-Quintana et al., 2026***). Developmentally, Zasp52 appears in the embryo first at myotendinous junctions and also at Z-bodies – clusters which later coalesce to form Z-discs (***Katzemich et al., 2013***). Zasp52 binds actin via its N-terminal PDZ domain plus a long C-terminal extension (***Liao et al., 2020***), and α-actinin via a region encompassing the PDZ domain plus a short C-terminal extension (***Liao et al., 2016***). In addition to the PDZ and Zasp motif (ZM) domain, Zasp52 contains four LIM domains, which interact with the ZM domain resulting in auto-oligomerization; this mechanism is believed to drive radial growth of the Z-disc, as well as pathological aggregate formation (***González-Morales et al., 2019***; ***Medina-Quintana et al., 2026***). Its primary human ortholog LDB3/ZASP is implicated in muscular dystrophies, which are characterized by progressive adult-onset distal myofibrillar myopathy and sometimes cardiomyopathy (***Griggs et al., 2007***).

Zasp52 is alternatively spliced into 22 different isoforms (according to FlyBase release FB2025_02, used throughout this paper), which leads to a variety of different domain and inter-domain combinations. The inter-domain linker regions connecting Zasp52's structured domains (i.e. PDZ, ZM, and LIM domains) are less characterized but are proposed to play an important role in protein function (***Fisher and Schöck, 2022***).

Though not much is known about the linker region between LIM1 and LIM2, its predominant expression in IFM and unusually large length prompted us to investigate it. We were curious to see how deleting only this linker region while retaining all conserved domains would affect muscle structure and function. This linker was found to be highly disordered; intrinsically disordered regions (IDRs) have mostly been analyzed biochemically, with only limited data on their in vivo function in model organisms (***Jensen et al., 2025***). Flight ability was impaired and myofibrils displayed a variety of phenotypes, which were all indicative of a loss of thin filament anchoring at the Z-disc. Most phenotypes exhibited an age-related increase in severity. Put together, these data demonstrate a crucial role for this large IDR in maintaining sarcomere integrity by stabilizing thin filaments at the Z-disc in IFM.

Results

exon 15e-containing isoforms are expressed in a specific spatiotemporal manner

Zasp52 isoforms containing the first and second LIM domains contain a linker region between the two, which can vary greatly in size. Encoded by several exons, this linker region may contain exon 15, which undergoes alternative 5′ splice site selection, generating five exonic variants (15a–e) ranging from 130 nucleotides (15a) to 4429 nucleotides (15e) in length (***Figure 1A***). The last 29 nucleotides of exon 15 contribute to the second LIM domain, but the remainder encodes the linker. When exon 15e is included, it constitutes the majority of the entire protein, encoding 1475 amino acids, which total 160 kDa. In the canonical and longest isoform Zasp52-PF, the entire protein is 2194 amino acids long, and the linker region between LIM1 and LIM2 is 1686 amino acids long. Exon 15e is referred to variously by other sources: as exon 9 in Flybase, exon 16c in ***Katzemich et al., 2011***, exon 18/19 in ***Benna et al., 2009***; protein isoforms containing exon 15e were previously also referred to as Z(210) (***Chechenova et al., 2013***).

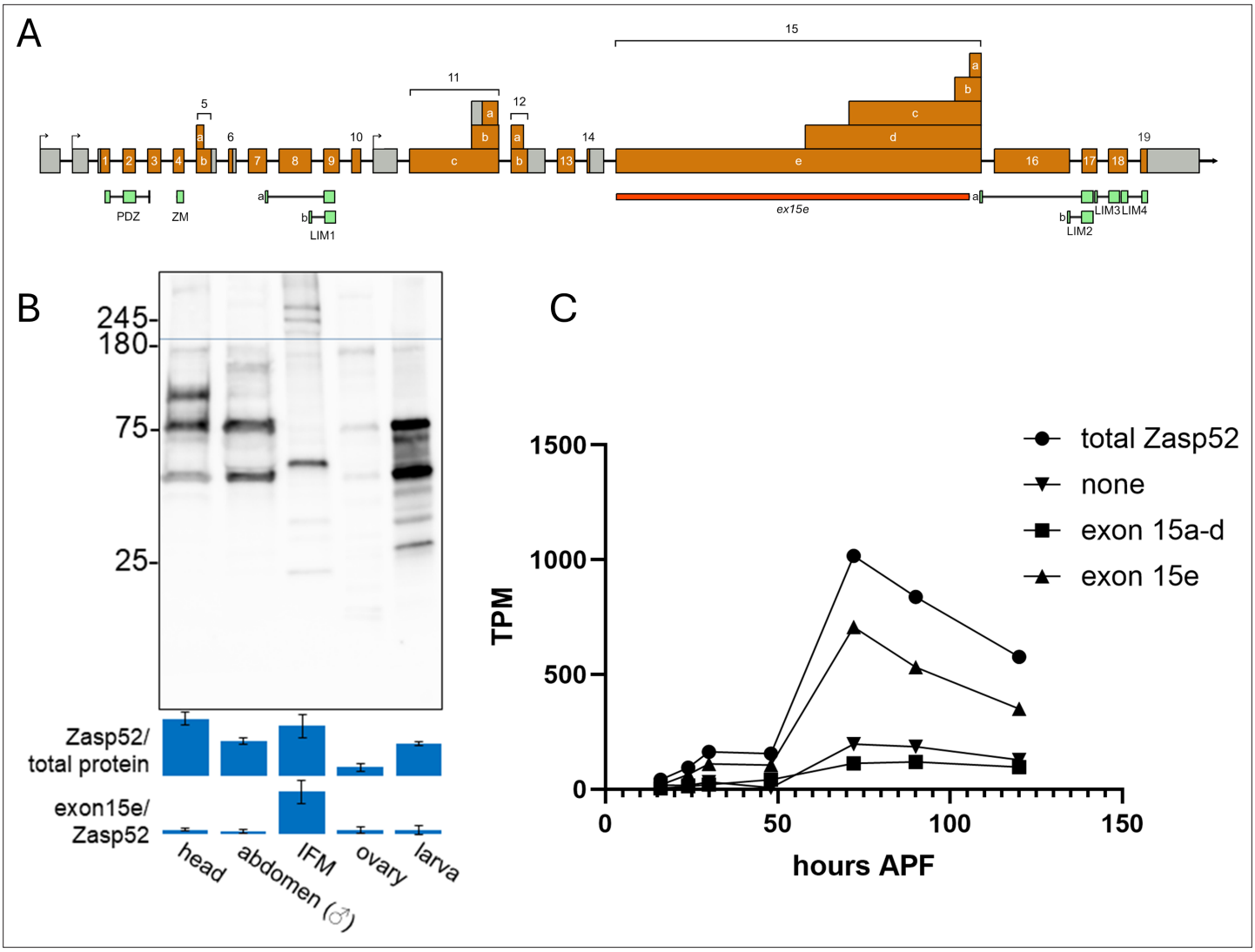

Figure 1. exon 15e-containing isoforms are expressed in a specific spatiotemporal manner. (**A**) A schematic of the *Zasp52* locus. Exons are drawn to scale; introns are not. Coding exons are shown in orange and untranslated regions in gray. Alternative start sites are also indicated. Below, in green, are mappings of structured domains according to SMART ***Letunic and Bork, 2018***; and also ***Katzemich et al., 2011***, which defined LIM1 and LIM2 variants. The deletion in *ex15e* mutants is indicated in red. (**B**) Western blot using five different tissue extracts from control flies probed with a Zasp52 full-length antibody. Relative amounts of Zasp52 content, as measured in each lane, over the total protein content, as measured using the TGX Stain-free gel method, are quantified below for each tissue as mean, with error bars representing standard deviation (n=3). Exon 15e content, as measured using the protein content above the dotted blue line for each lane, over Zasp52 content, is quantified below that. Molecular weights appear higher, perhaps due to retardation caused by non-specific interactions with the gel matrix, as also seen in ***Watts et al., 2017***. (**C**) RNA-seq data from ***Spletter et al., 2018***, of indirect flight muscle (IFM) tissue across various timepoints after puparium formation; the last timepoint is of adults 1 day after eclosion. Gene expression levels in transcripts per million (TPM) are shown for Zasp52 isoforms classified according to their splicing of exon 15. The majority of Zasp52 IFM isoforms contain exon 15e.

The online version of this article includes the following source data and figure supplement(s) for figure 1:

Source data 1. PDF file containing the original western blot for ***Figure 1B***, with relevant bands indicated.

Source data 2. Original TIF file of western blot displayed in ***Figure 1B***.

Figure supplement 1. RNA-seq data of exon 15e expression.

Figure supplement 2. Disorder prediction of amino acids encoded by exon 15e.

Western blotting using a polyclonal antibody capable of detecting all Zasp52 splice variants (hereinafter referred to as the Zasp52 full-length antibody, ***Jani and Schöck, 2007***) was used to analyze the presence of Zasp52 in IFM, ovaries, whole larvae, heads, and whole male abdomens (***Figure 1B***). IFM contains the second most Zasp52 protein of any isoform relative to total protein content compared to the other tissues analyzed and is the only tissue that significantly contains exon 15e-containing isoforms relative to total Zasp52 content. This agrees with previous studies (***Chechenova et al., 2013***; ***Benna et al., 2009***), which found no higher weight isoforms in larvae, and with transcriptomics data. Whole organism RNA-seq data from the ENCODE project (***Duff et al., 2015***) reveals very little expression of exon 15e in all developmental stages up until 4 days past the white prepupal stage (***Figure 1—figure supplement 1***). To verify that this is indeed a phenomenon of exon 15e inclusion and not merely Zasp52 expression, one can look at the surrounding exons, which do not follow the same pattern as exon 15e. To gain a more precise perspective on IFM expression of exon 15e, we turned to an RNA-seq dataset from ***Spletter et al., 2018***, which looked at total RNA content of IFM at various developmental time points (***Figure 1C***). Expression of all Zasp52 transcripts in IFM surges from 48 to 72 hr after puparium formation (APF), with most of these transcripts containing exon 15e, as opposed to including exon 15a–d only or no exon 15 at all.

We used various software to predict the level of disorder across Zasp52-PF (***Figure 1—figure supplement 2A***). All identified the linker region between LIM1 and LIM2 as an IDR to various degrees, although some regions within it appear more ordered. The actin-binding motif (ABM) identified by ***Ashour et al., 2023***, within exon 15e is predicted to be more structured than the surrounding regions. No significant sequence similarity was found when aligning Zasp52's linker region to human or other *D. melanogaster* ALP/Enigma protein family members. We then compared the lengths of the linker regions between LIM1 and LIM2 in all insect species possessing a Zasp52 ortholog as defined by NCBI's Eukaryotic Genome Annotation Pipeline (***Figure 1—figure supplement 2B***). Drosophilids generally have a longer linker than their taxonomical neighbors. Mayflies, dragonflies, and damselflies, which use direct flight muscle, have notably short linkers. Since linear sequence often does not fully describe an IDR's function, we analyzed linear clustering or mixing of different residue types using NARDINI (***Cohan et al., 2022***). The z-score matrix of the linker region between LIM1 and LIM2 in Zasp52-PF showed a strong clustering/segregation of polar residues (μ), as well as alanine (A) and proline (P), and hydrophobic residues (h) (***Figure 1—figure supplement 2C***). The z-score matrix of exon 15e alone displayed much of the same clustering, except with additional strong clustering of acidic residues (-) with respect to other residue classes (***Figure 1—figure supplement 2C'***). This implies that the additional exons in the linker region dilute or mask the strong clustering of acidic residues in exon 15e alone. We attempted to compare z-score matrices across various arthropod species but were unable to detect any meaningful correlation, indicating that the binary patterns uncovered by NARDINI do not reveal taxonomical differences in exon 15e composition.

A CRISPR deletion of exon 15e displays flight defects

To further investigate the function of exon 15e, we generated a CRISPR deletion spanning five intronic nucleotides 5′ to exon 15e up to 149 nucleotides before the 3′ end of exon 15e (***Figure 1A***). In total, 4285 nucleotides totaling 156 kDa were deleted. Thus, our mutants would affect all isoforms containing exons 15b–e. The deletion endpoints were sequenced to confirm effective CRISPR knockout. To confirm that our deletion worked and spliced as intended, we performed western blots using the Zasp52 full-length antibody to compare our deletion with a control and the MiMIC line *MI00979* (***Venken et al., 2011***), which truncates everything C-terminal to and including exon 15e (***Figure 2A***). The largest protein that could possibly be present in our mutant would be 136 kDa (Zasp52-PI). Our deletion was devoid of all higher-molecular-weight isoforms containing exon 15e, which were present in the control as expected. Our deletion also contained several isoforms that were heavier than the highest molecular weight isoforms of *MI00979,* which were also not present in control, suggesting that these are novel products containing the C-terminal LIM domains. To confirm that this was indeed the case, i.e., that the three C-terminal LIM domains were retained, we raised an antibody against them and performed a western blot (***Figure 2A'***). Our CRISPR deletion retained these LIM domains as expected. We refer to this CRISPR mutant as *ex15e*.

We wanted to see how *ex15e* affected the locomotory abilities of the fly. Since larvae do not express exon 15e, we do not expect them to be affected by our deletion. Therefore, we performed

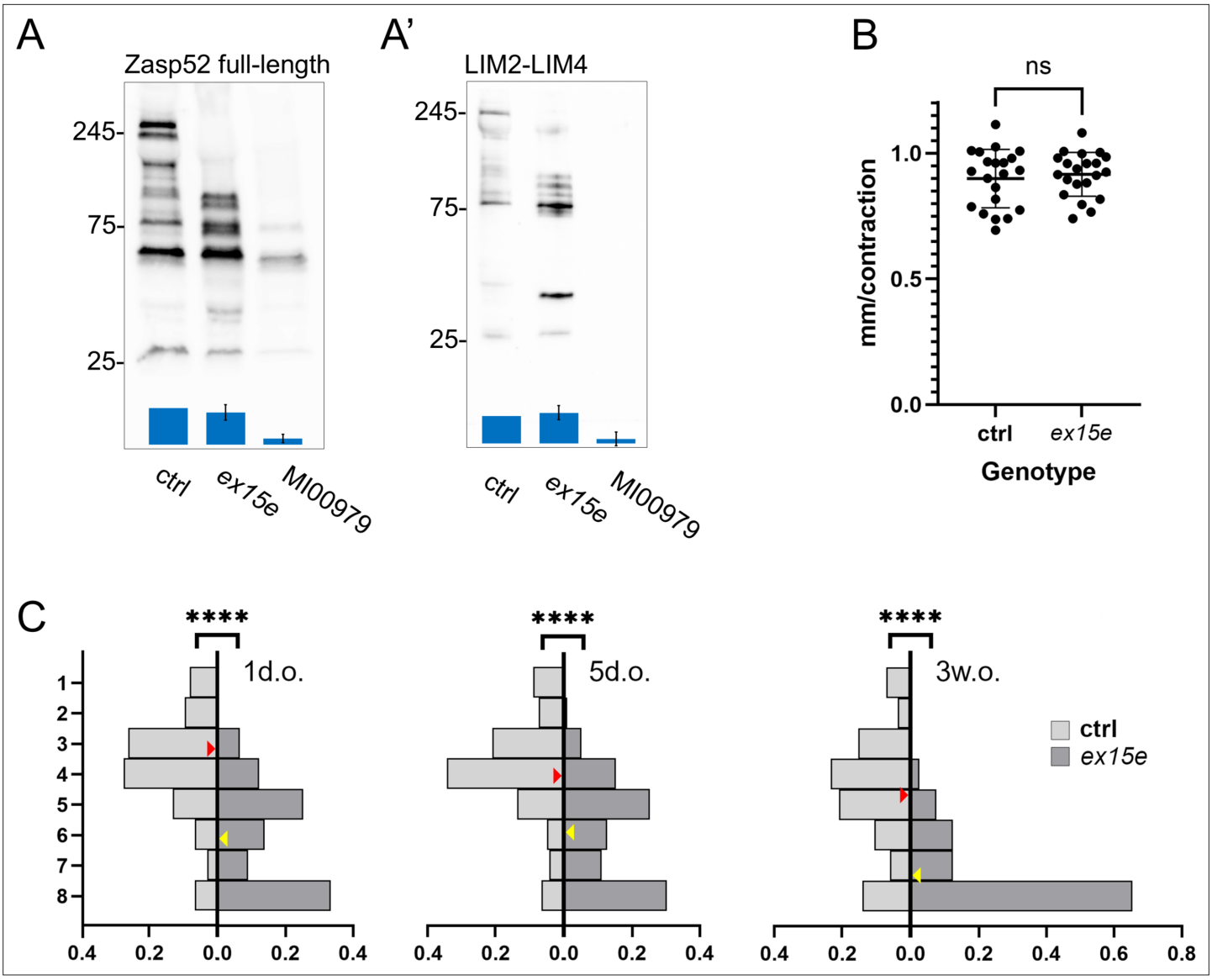

Figure 2. A CRISPR deletion of exon 15e displays flight defects. Western blots using either the Zasp52 full-length antibody (**A**) or antibody against LIM2-LIM4 (**A'**) of either w^{1118} (ctrl hereinafter), *ex15e*, or the MiMIC line *MI00979* whole flies. Relative amounts of Zasp52 content, as measured in each lane, over the total protein content, are quantified below for each genotype as mean with error bars representing standard deviation (*n*=3) normalized against the ctrl lane. (**B**) Larval crawling assay of either ctrl (*n*=21) or *ex15e* (*n*=21) third instar larvae showing no significant difference between the two (unpaired t-test with Welch's correction; p=0.6006). (**C**) Flight assays of ctrl versus *ex15e* flies of three different age categories: 1-day-old (ctrl *n*=138 flies, *ex15e* *n*=123), 5-days-old (ctrl *n*=125, *ex15e* *n*=119), and 3-weeks-old (ctrl *n*=86, *ex15e* *n*=81). The y-axis indicates flight strength: flies were released into a tube and those that landed in the top segment (y=1) had the strongest flight strength while those that landed in the bottom dish (y=8) had the weakest. The x-axis indicates the proportion of flies that landed in that segment. Red arrows indicate the average position landed in ctrl flies; yellow arrows are for *ex15e* flies. Difference in flight ability was statistically significant for all age categories (Fisher's exact test; p<0.0001).

The online version of this article includes the following source data and figure supplement(s) for figure 2:

Source data 1. PDF file containing the original western blots of ***Figure 2A and A'***, with relevant bands indicated.

Source data 2. Original TIF files of western blots displayed in ***Figure 2A and A'***.

Figure supplement 1. Flight assays, gross muscle morphology, and modified terminal Z-discs in *ex15e* mutant.

a larval crawling assay as a negative control to confirm that *ex15e* larval muscles were unaffected (***Figure 2B***). As predicted, control and *ex15e* larvae demonstrated no differences in crawling ability. Next, we wanted to see how flight would be affected, given that exon 15e is present primarily in the adult IFM. *ex15e* flies of all age categories had impaired flight ability compared to control with a

severe deterioration at 3 weeks of age (***Figure 2C***). To ensure that no secondary-site mutations were affecting our mutant phenotypes, we performed a simple binary flight assay using the heterozygous *ex15e* deletion over a Zasp52 deficiency (***Figure 2—figure supplement 1A***).

This impairment in flight could stem from a variety of causes, given the multimodal functionality of Zasp52. We decided to first look at gross muscle morphology before zooming in on our investigation. Thorax bisections revealed no noticeable difference in the IFMs of *ex15e* and control flies (***Figure 2—figure supplement 1B, C***). Since Zasp52 was known to be involved in integrin interactions (***Jani and Schöck, 2007***; ***Bouaouina et al., 2012***) and junctional components (***Ashour et al., 2023***), we inspected the myotendinous junctions of IFM, which are called modified terminal Z-discs (MTZ), in 3-week-old flies (***Figure 2—figure supplement 1D–G″***). βPS integrin localization appeared unaffected in *ex15e*; this agrees with integrins being upstream of Zasp52 (***Jani and Schöck, 2007***). However, the MTZ appeared disrupted and malformed, lacking the organized structure seen in controls. Furthermore, we also noticed myofibril defects which prompted us to further investigate IFM at the myofibrillar level.

ex15e mutant IFM phenotypes: bending at the Z-disc and thin filament intrusion into the H-zone

IFM tissue was analyzed by confocal microscopy with several phenotypes being observed. First, myofibrils in *ex15e* mutants were often found to be bent at the Z-disc (***Figure 3A–C***). In control flies, sarcomeres across different age groups typically displayed the same proportion of degree of bentness. In *ex15e*, the proportion of bent sarcomeres increased with age, as well as the degree of bending, compared to control flies. Force-induced bending results in a sarcomere whose inner curve is bowed, much like a hose with a kink. The bending in *ex15e* appears to be a result of the improper anchoring of thin filaments, which leads to a shear type angle shift in the sarcomere at the Z-disc. Bending was found exclusively at the Z-disc and not the M-line in all muscle analyzed.

Another phenotype observed in *ex15e* was the presence of a dense band of actin staining at the H-zone, where normally there would be no actin staining (***Figure 3D–F***). Control flies have very few sarcomeres with this phenotype at all ages; *ex15e* are similar to control at 1 day of age but begin to accumulate a large number of these abnormal sarcomeres with time. At 3 weeks of age, a large proportion of sarcomeres have actin at the H-zone. Usually, groups of myofibrils in the same area would exhibit this phenotype rather than these abnormal myofibrils being randomly dispersed among the normal ones. This dense band of actin suggested that thin filaments were overlapping at the M-line. This could be a result of hypercontraction, where thin filaments are brought so close together that they overlap. However, the protocol used for these preparations includes a relaxing solution containing ATP, which induces cross-bridge detachment resulting in the adoption of a relaxed conformation. To see if these abnormal sarcomeres with actin in the H-zone were indeed contracted, we measured their length and compared them to normal sarcomeres from the same sample in 3-week-old flies (***Figure 3G***). Sarcomeres with actin in the H-zone had a smaller length than those without, indicating that they were indeed contracted. Muscle decontraction relies on the elastic nature of the sarcomere to restore it to a relaxed conformation once myosin heads detach from the thin filaments. This requires stable Z-discs and myofilament attachments, the lack of which may be the cause of a permanent hypercontracted state in *ex15e*.

To further investigate these phenomena, we performed transmission electron microscopy (TEM) of myofibrils and noticed phenotypes that concurred with our immunofluorescence analysis. Wild-type IFM sarcomeres of 3-week-old flies are highly stereotypic with electron-dense, continuous Z-discs, and regular H-zones (***Figure 4A***). In contrast, *ex15e* mutants show low-density, discontinuous Z-discs with many gaps, as well as irregular H-zones (***Figure 4B***). We also observed bent Z-discs and split myofibrils, as well as fraying of filaments at the sarcomere periphery (***Figure 4C***). The latter two phenotypes could also be observed in transverse sections of myofibrils (***Figure 4D***). Altogether, these observations indicate a breakdown of Z-disc coherence and stability leading to additional downstream effects such as myofibril splitting and fraying.

A putative ABM within exon 15e is not responsible for *ex15e* defects

A putative F-actin binding motif (ABM) identified by ***Ashour et al., 2023***, is located within exon 15e and might be responsible for the thin filament-related phenotypes we witnessed in *ex15e* (see ***Figure 1—figure supplement 2A*** for location). This short motif found in the CapZbeta protein of

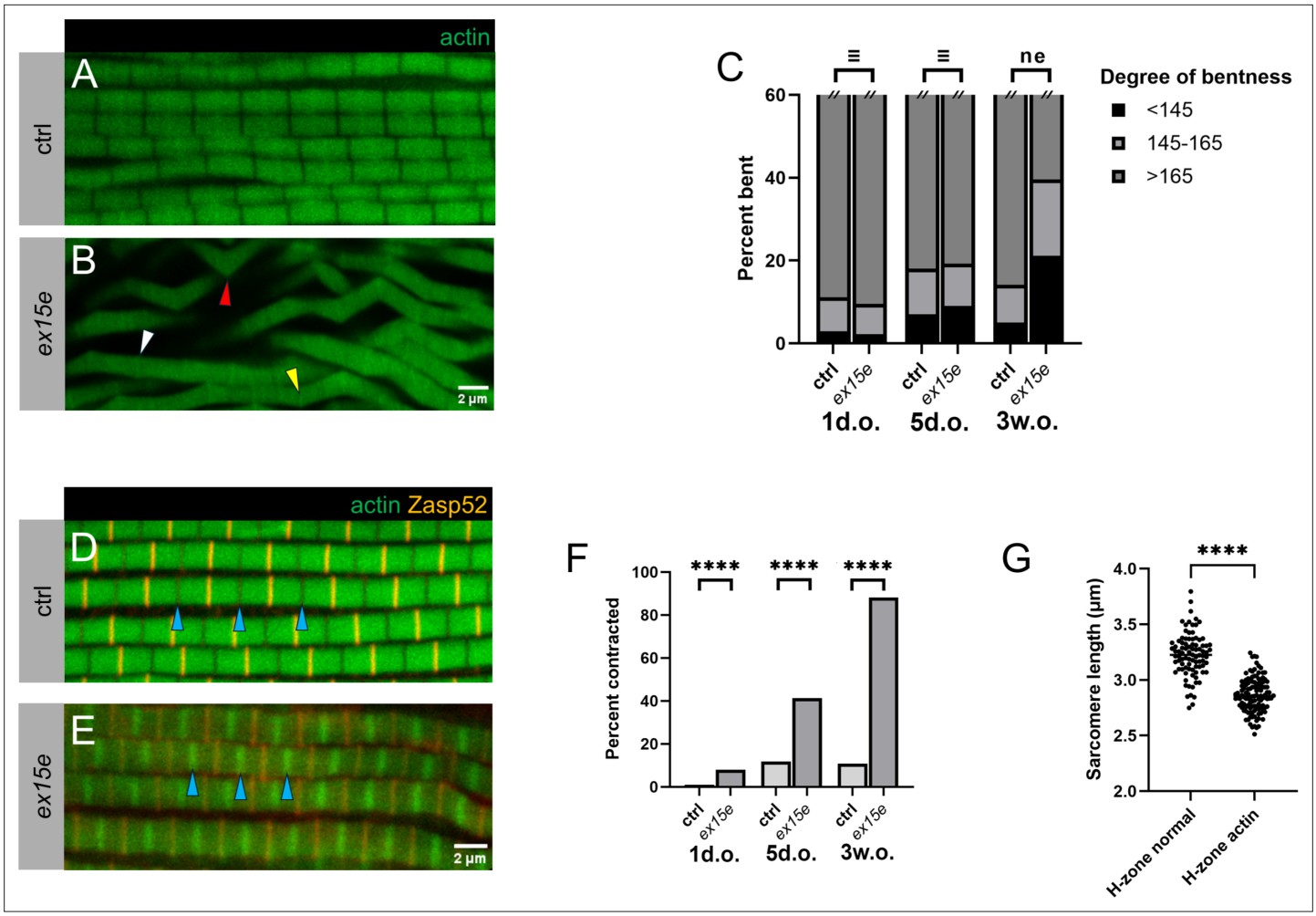

Figure 3. *ex15e* mutant indirect flight muscle (IFM) phenotypes: bending at the Z-disc and thin filament intrusion into the H-zone. (**A–C**) Analysis of bent sarcomere phenotype. Actin is visualized by phalloidin in green. Ctrl myofibrils (**A**) appear straight while *ex15e* myofibrils (**B**) contain a range of bending (representative 3-week-old myofibrils shown). Red arrowhead indicates a representative sarcomere with a bend of <145°, yellow arrowhead indicates 145–165°, and white arrowhead >165°. (**C**) Bend angles were statistically equivalent (≡) between ctrl and *ex15e* in 1-day-olds and 5-day-olds, but not equivalent (ne) in 3-week-olds, where *ex15e* displayed greater bentness. Sample sizes: 1-day-old (ctrl *n*=1242 sarcomeres, *ex15e n*=1851), 5-days-old (ctrl *n*=1192, *ex15e n*=946), and 3-weeks-old (ctrl *n*=1768, *ex15e n*=1125) (two one-sided test [TOST] with ±4.5° equivalence margin, α=0.05; 1d.o. t_L = 12.95, t_U = −12.07; 5d.o. t_L = 6.03, t_U = −8.01; 3 w.o. t_L = −6.34, t_U = −20.63). (**D–F**) Sarcomeres also exhibited actin in the H-zone phenotype (representative 3-week-old myofibrils shown). Ctrl myofibrils (**D**) display normal H-zones without actin, with M-lines/H-zones indicated by blue arrowheads. *ex15e* myofibrils (**E**) display actin accumulation at the H-zone; arrowheads indicate same as above. Actin is visualized by phalloidin in green and Z-discs are identified by the full-length Zasp52 antibody in red. (**F**) These sarcomeres with H-zone actin, which appear hypercontracted, are significantly overrepresented in *ex15e* compared to ctrl across all age categories. Sample sizes were as follows: 1-day-old (ctrl *n*=3255 sarcomeres, *ex15e n*=4056), 5-days-old (ctrl *n*=3221, *ex15e n*=2677), and 3-weeks-old (ctrl *n*=5394, *ex15e n*=4720) (Fisher's exact test; p<0.0001). (**G**) To ascertain that sarcomeres with actin in the H-zone were indeed contracted, the Z- to Z-disc length was measured in *ex15e* 3-week-old flies of both sarcomeres with a bare H-zone (H-zone normal, *n*=89 sarcomeres) and those with actin in the H-zone (H-zone actin, *n*=117). H-zone actin sarcomeres were significantly smaller (unpaired t-test with Welch's correction; p<0.0001).

various metazoans is present in the Zasp52 proteins of the *D. melanogaster* subgroup (***Ashour et al., 2023***). To test the role of this ABM, we used CRISPR to delete five amino acids (LQREL), which include two highly conserved leucines, and confirmed the in-frame deletion by sequencing – we refer to this mutant as *ΔABM*. Myofibrils appear normal (***Figure 5A–C***) and do not display the abnormal bending (***Figure 5D***) and contraction (***Figure 5E***) of *ex15e*. Flight ability distributions are slightly different from control flies, although the average flight index is almost identical (***Figure 5F***). In conclusion, *ΔABM* does not phenocopy *ex15e*, which indicates that exon 15e's function is not reducible to that short motif. Instead, the IDR is essential for the phenotypes we observed.

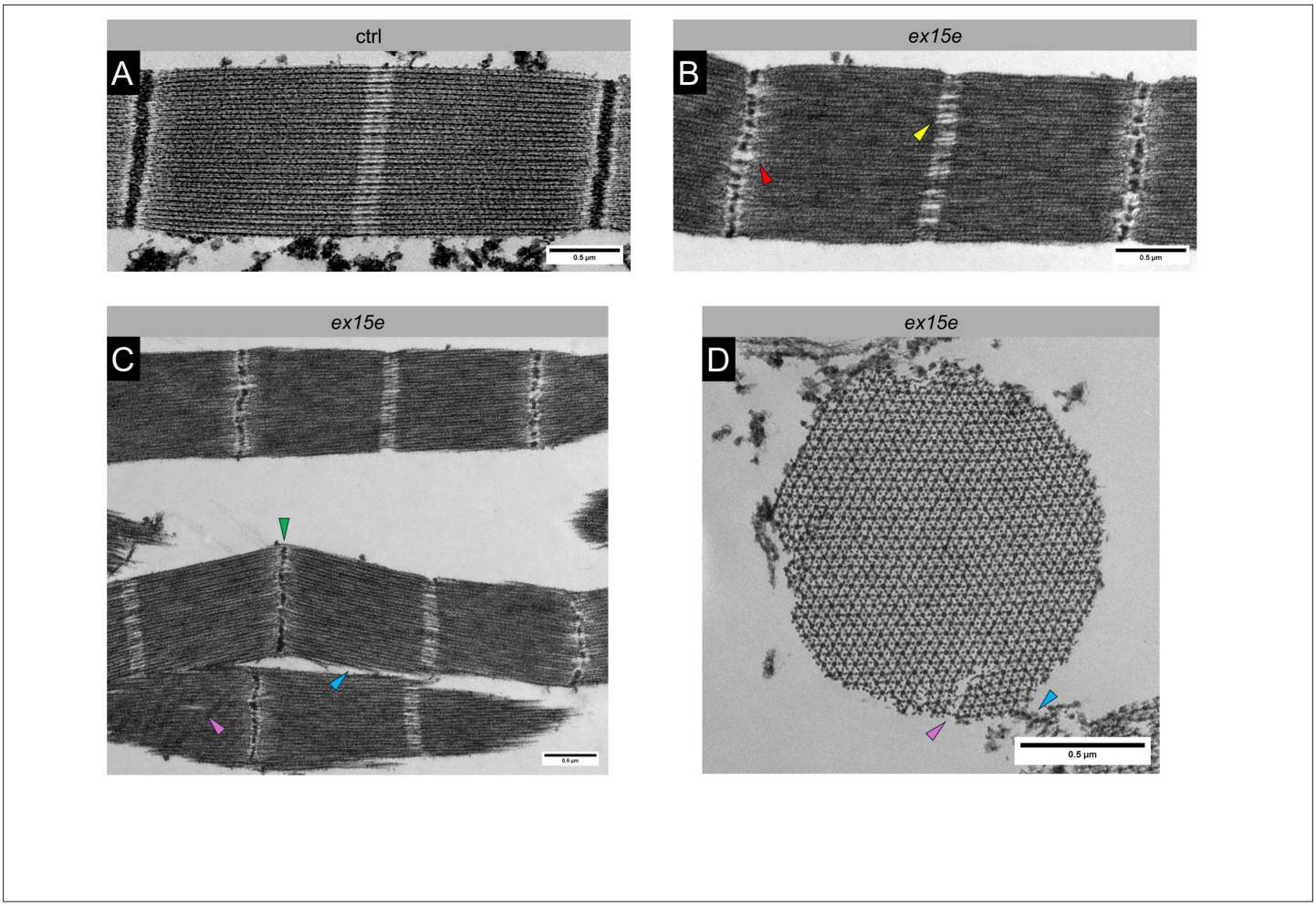

Figure 4. Transmission electron microscopy (TEM) reveals defects in mutant sarcomere ultrastructure. TEM images reveal similar phenotypes as immunofluorescent ones (3-week-old shown). Ctrl (**A**) sarcomeres are very structured and even. Longitudinal sections of *ex15e* (**B, C**) display broken Z-discs (red arrowhead), broken M-lines (yellow arrowhead), bending at the Z-discs (green arrowhead), splits in filaments (purple arrowhead), and fraying of peripheral filaments (blue arrowhead). Transverse sections of *ex15e* (**D**) also display some of these abnormalities (purple and blue arrowhead).

ex15e defects are restored by rescue constructs

To determine if the phenotypes are truly due to the IDR or are caused by an altered isoform composition, we wanted to see if the phenotypes of *ex15e* could be rescued with two different isoforms: Zasp52-PF is the canonical full-length Zasp52 isoform which contains exon 15e, while Zasp52-PR contains all structured domains but not exon 15e (***Figure 6A***). We expressed either UAS-Zasp52-PF or UAS-Zasp52-PR using the UH3-GAL4 driver in a homozygous *ex15e* background and examined 3-week-old flies (***Figure 6B–H***). UH3-GAL4 is expressed in IFM from 36 hr APF into adulthood (***Singh et al., 2014***). The degree of bending in Zasp52-PR rescue sarcomeres was statistically equivalent to that of *ex15e* mutants, while that of Zasp52-PF rescues was equivalent to control flies, indicating that Zasp52-PF but not Zasp52-PR can rescue this phenotype (***Figure 6F***). The proportion of H-zone actin (i.e. hypercontracted) sarcomeres was not significantly different between *ex15e* and Zasp52-PR rescues as expected. Interestingly, no hypercontracted sarcomeres were observed upon re-expression of Zasp52-PF, again indicating a successful rescue (***Figure 6G***). Finally, we tested flight ability and observed a significant increase in flight strength in Zasp52-PF rescues compared to Zasp52-PR rescues, with the latter being not significantly different from *ex15e* (***Figure 6H***). Zasp52-PF rescues were still weaker fliers than control flies, suggesting a partial rescue of flight ability. Overall, only a transgene containing exon 15e resulted in rescue, showing that the phenotypes are due to the IDR.

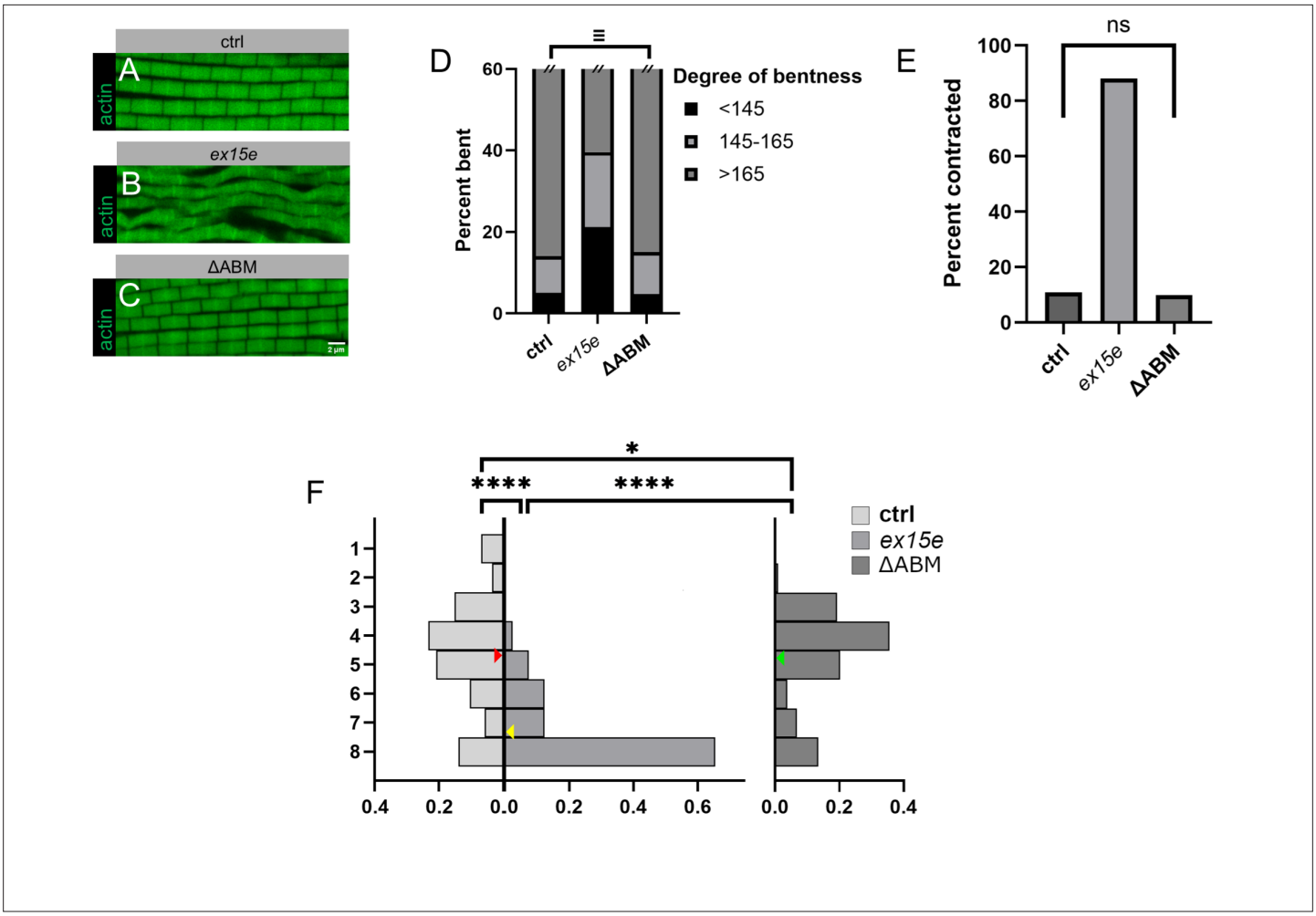

Figure 5. A putative actin-binding motif within exon 15e is not responsible for *ex15e* defects. *ΔABM* homozygotes along with all other flies in this figure were analyzed at 3 weeks of age. *ΔABM* myofibrils (**C**) resembled those of ctrl (**A**) and showed none of the phenotypes seen in *ex15e* mutants (**B**). Actin is visualized by phalloidin in green. (**D**) Bend angles were equivalent between ctrl and *ΔABM* flies (n=1648) (two one-sided test [TOST] with ±4.5° equivalence margin, α=0.05; t_L = 21.88, t_U = −7.93). (**E**) The proportion of sarcomeres that were contracted was not significantly different between ctrl and *ΔABM* flies (n=3773) (Fisher's exact test; p=0.1274). (**F**) Flight ability was only slightly decreased in ΔABM flies (n=104 flies) compared to ctrl (n=86) but significantly improved compared to *ex15e* (n=81). Red arrows indicate the average position landed in ctrl flies, yellow are *ex15e*, and green are *ΔABM* (Fisher's exact test; ctrl-*ΔABM* p=0.0351; ctrl-*ex15e* and *ex15e*-*ΔABM* p<0.0001).

ex15e and actin genetically interact

We next wanted to test for a genetic interaction between exon 15e and Act88F (the actin isoform present in IFM) by analyzing heterozygous *ex15e*, heterozygous *Act88F*^{KM88} (an amorphic mutant of *Act88F*), and a di-heterozygous combination of both (*ex15e*/+; *Act88F*^{KM88}/+) (***Figure 7A–D***). *ex15e*/+ resembled control myofibrils, and *Act88F*^{KM88}/+ has mild myofibrillar defects. *ex15e*/+; *Act88F*^{KM88}/+ exhibited supra-additive effects where we often noticed a novel phenotype of very large H-zones. A ratio of twice the thin filament length to the total sarcomere length was computed for all genotypes. Lower values represented sarcomeres whose thin filaments occupied a smaller proportion of the sarcomere and consequently had larger H-zones, whereas a value of one represented the absence of an H-zone. This ratio was not significantly different between control, *ex15e*/+, and *Act88F*^{KM88}/+, but was considerably smaller in di-heterozygotes (***Figure 7E***), indicating a strong genetic interaction between Act88F and exon 15e.

FRAP reveals defects in *ex15e* protein dynamics

We decided to test whether exon 15e could localize to the Z-disc on its own. To do this, we expressed the GFP-tagged exon 15e using the UH3-GAL4 driver (UH3>GFPexon15e). We observed successful

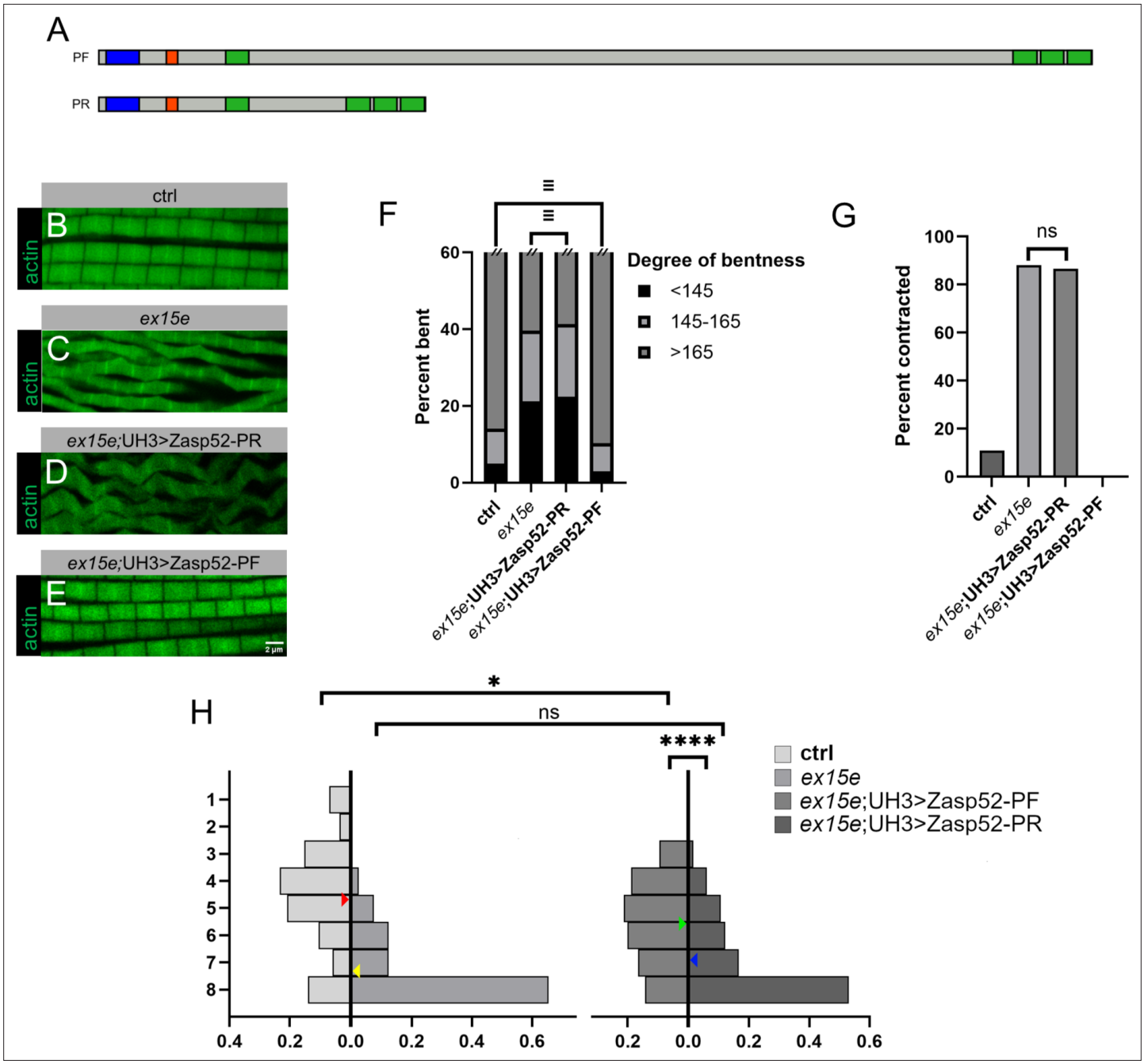

Figure 6. *ex15e* defects are restored by rescue constructs. Zasp52-PF or Zasp52-PR was heterozygously overexpressed with a UH3-GAL4 driver in a homozygous *ex15e* background in a rescue attempt. In this figure, all myofibrils had actin visualized with phalloidin in green. All experiments were done at 3 weeks of age, and ctrl and *ex15e* data are the same as previous. (**A**) Schematic showing Zasp52-PF, which is the canonical full-length isoform, and Zasp52-PR, which contains all structured domains but lacks exon 15e. PDZ domain (blue), ZM (red), LIM domains (green). (**B–E**) Myofibrils display bending, Z-disc disruption, and overall myofibrillar disorganization in Zasp52-PR overexpressions (**D**), similar to *ex15e* (**C**), while Zasp52-PF overexpression (**E**) appears similar to ctrl (**B**). (**F**) Bend angles were equivalent (≡) between *ex15e* and *ex15e*; UH3>Zasp52-PR, and between ctrl and *ex15e*; UH3>Zasp52-PF. Sample sizes: *ex15e*; UH3>Zasp52-PR n=2049 sarcomeres, *ex15e*; UH3>Zasp52-PF n=2221 (two one-sided test [TOST] with ±4.5° equivalence margin, α=0.05; *ex15e-ex15e*; UH3>Zasp52-PR t_L = 1.92, t_U = −10.16; ctrl-*ex15e*; UH3>Zasp52-PF t_L = 17.65, t_U = −8.51). (**G**) The proportion of sarcomeres that were contracted (i.e. actin in H-zone) was not significantly different between *ex15e* and *ex15e*; UH3>Zasp52-PR, whereas no such sarcomeres were found in *ex15e*; UH3>Zasp52-PF. Sample sizes: *ex15e*; UH3>Zasp52-PR n=2843 sarcomeres, *ex15e*; UH3>Zasp52-PF n=2480 (Fisher's exact test; p=0.0521). (**H**) Flight ability was significantly improved in *ex15e*; UH3>Zasp52-PF (n=85) compared to *ex15e*; UH3>Zasp52-PR (n=66), with *ex15e*; UH3>Zasp52-PR showing no significant difference from *ex15e* but *ex15e*; UH3>Zasp52-PF showing a significant difference from ctrl. Red arrows indicate the average position landed in ctrl flies, yellow are *ex15e*, blue are *ex15e*; UH3>Zasp52-PR, and green are *ex15e*; UH3>Zasp52-PF

Figure 6 continued on next page

Figure 6 continued

(Fisher's exact test; *ex15e*; UH3>Zasp52-PR-*ex15e*; UH3>Zasp52-PF p<0.0001; *ex15e-ex15e*; UH3>Zasp52-PR p=0.2668; ctrl-*ex15e*; UH3>Zasp52-PF p=0.0129).

localization to the IFM Z-discs (***Figure 8A***) and thus decided to assess kinetics using fluorescence recovery after photobleaching (FRAP). One-day-old IFM Z-discs were photobleached, and recovery of fluorescence was monitored. Compared to GFP-tagged Zasp52-PR (UH3>GFPZasp52-PR), which lacks exon 15e, exon15e-GFP displayed much lower recovery over a 96 s period (***Figure 8B***). This suggests that the IDR stabilizes Zasp52 at the Z-disc and reduces its turnover. We then expressed GFP-tagged Zasp52-PR, which cannot rescue (see ***Figure 6***), in an *ex15e* background (*ex15e*; UH3>GFPZasp52-PR). Fluorescence recovery in the *ex15e* background was to a significantly higher level compared to the wild-type background (***Figure 8C***), resulting in a larger mobile fraction (***Figure 8D***). A greater mobile fraction in our mutant background confirms that the IDR is required to hold Zasp52 in place at the Z-disc, either by fastening itself, and/or keeping other molecules in place thereby contributing to overall Z-disc stability.

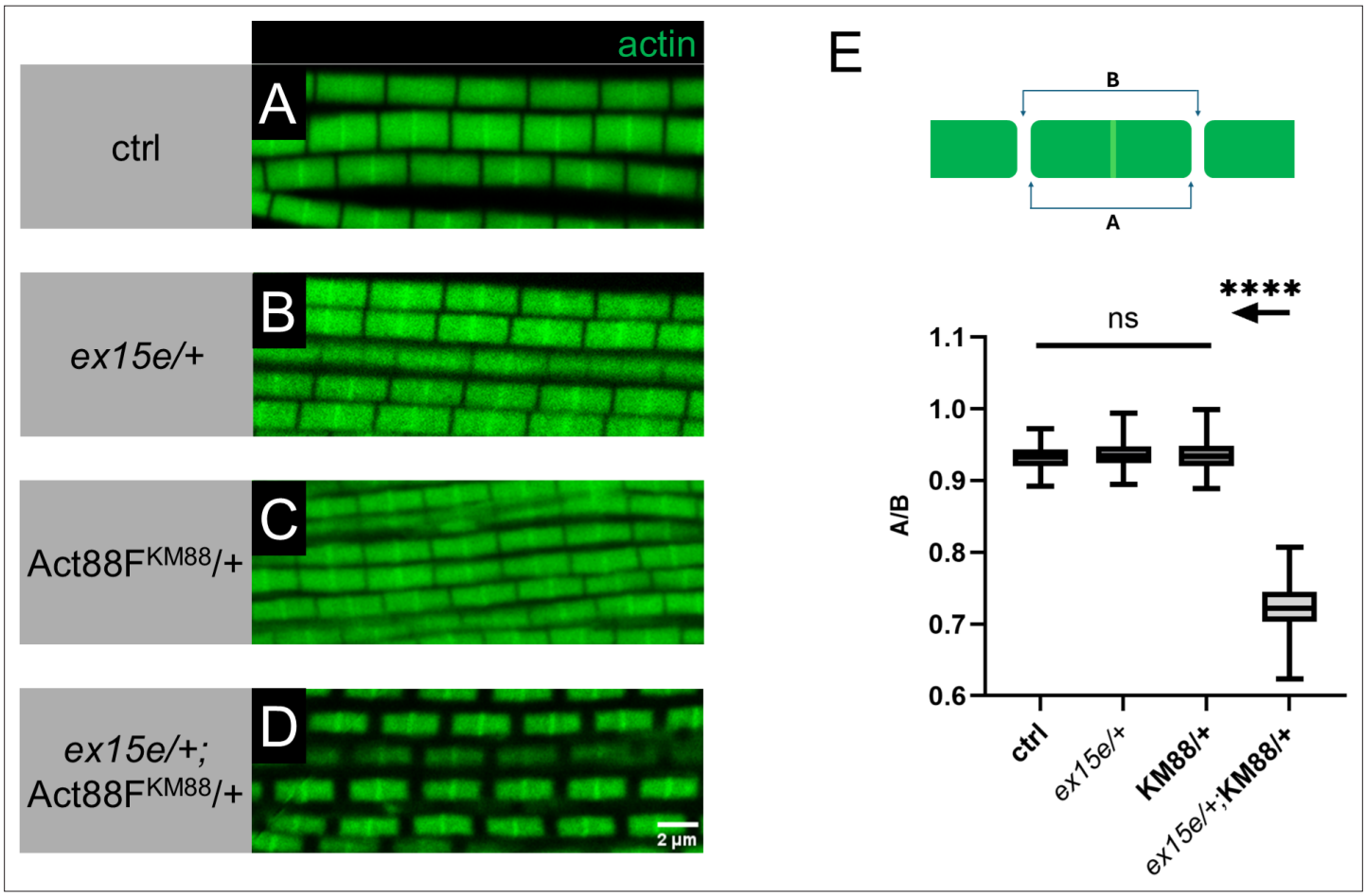

Figure 7. Large H-zones demonstrate a genetic interaction between exon 15e and Act88F. (**A–D**) Myofibrils of 1-day-old flies of various genotypes. Actin was visualized with phalloidin in green. Ctrl (**A**) and heterozygous *ex15e* myofibrils (**B**) appear indifferentiable; heterozygous *Act88F*^{KM88} (**C**) are slightly disrupted with fraying and slight narrowing. Representative *ex15e*/+; *Act88F*^{KM88}/+ myofibrils (**D**) with large H-zones are shown. (**E**) We quantified the ratio of twice the thin filament length denoted distance 'A' to the corresponding sarcomere's length denoted as 'B' for all four genotypes. A schematic illustrates the measurement of these distances. Sample sizes were as follows: ctrl *n*=119 sarcomeres, *ex15e*/+ *n* = 122, *Act88F*^{KM88}/+ *n* = 119, *ex15e*/+; *Act88F*^{KM88}/+ *n* = 119. The ratio A/B represents the proportion of the sarcomere length occupied by thin filaments and is inversely correlated with H-zone length; *ex15e*/+; *Act88F*^{KM88}/+ sarcomeres have significantly larger H-zones than all others (unpaired t-test with Welch's correction; ctrl-*ex15e*/+ p=0.0502; ctrl-*Act88F*^{KM88}/+ p=0.2770; ctrl-*ex15e*/+; *Act88F*^{KM88}/+ p<0.0001; *ex15e*/+-*Act88F*^{KM88} p=0.4938; *ex15e*/+-*ex15e*/+; *Act88F*^{KM88} p<0.0001; *Act88F*^{KM88}/+- *ex15e*/+; *Act88F*^{KM88} p<0.0001). All sarcomeres with an *Act88F*^{KM88} allele were radially narrower than ctrl, but a synthetic enhancement could not be concluded from this observation.

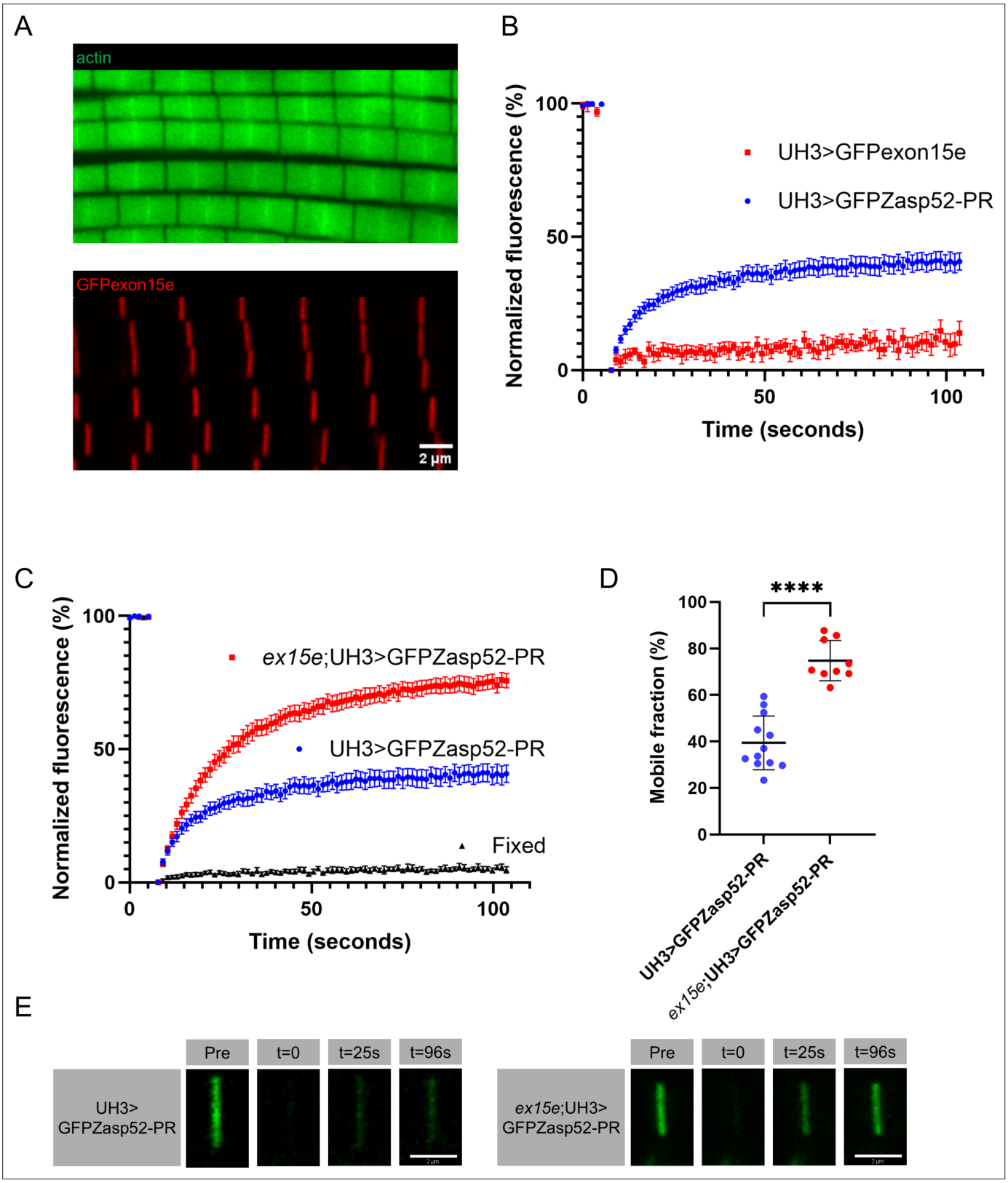

Figure 8. Fluorescence recovery after photobleaching (FRAP) reveals defects in *ex15e* protein dynamics. (**A**) GFP-tagged exon 15e localized to the indirect flight muscle (IFM) Z-discs in 1-day-old females. (**B**) FRAP experiments visualizing recovery of either GFP-tagged exon 15e (UH3>GFPexon15e, *n*=8) or GFPZasp52-PR (UH3>GFPZasp52-PR, *n*=12) were performed on 1-day-old female IFM Z-discs. (**C**) Recovery of GFPZasp52-PR was also assessed in 1-day-old female IFM Z-discs either in our mutant background (*ex15e*;UH3>GFPZasp52-PR, *n*=9 flies) or wild-type background (same data as in

Figure 8 continued on next page

Figure 8 continued

B). Ctrl UH3>GFPZasp52-PR Z-discs fixed with 4% paraformaldehyde for 10 min (labeled 'Fixed', *n*=7) displayed no recovery as expected. (**D**) Plateaus of fitted curves were significantly different, with a greater mobile fraction in the mutant background (unpaired t-test with Welch's correction; p<0.0001). (**E**) Representative snapshots of bleached Z-disc recovery illustrate this difference between genotypes.

ex15e defects are rescued by immobilization

On a different note, we noticed that virtually all the *ex15e* phenotypes worsened with age, which suggests that use might contribute to deterioration. We therefore decided to prevent flies from using their IFMs by immobilizing them. Flies were reared until 3 weeks of age in between glass plates separated by 1.5 mm spacers, which prevented them from flying or even attempting to fly. Myofibrils appear normal in immobilized *ex15e* mutant flies (***Figure 9A–C***). The degree of bending in immobilized flies was equivalent to that of control flies (***Figure 9D***). The proportion of hypercontracted sarcomeres was also not significantly different between immobilized and control flies (***Figure 9E***).

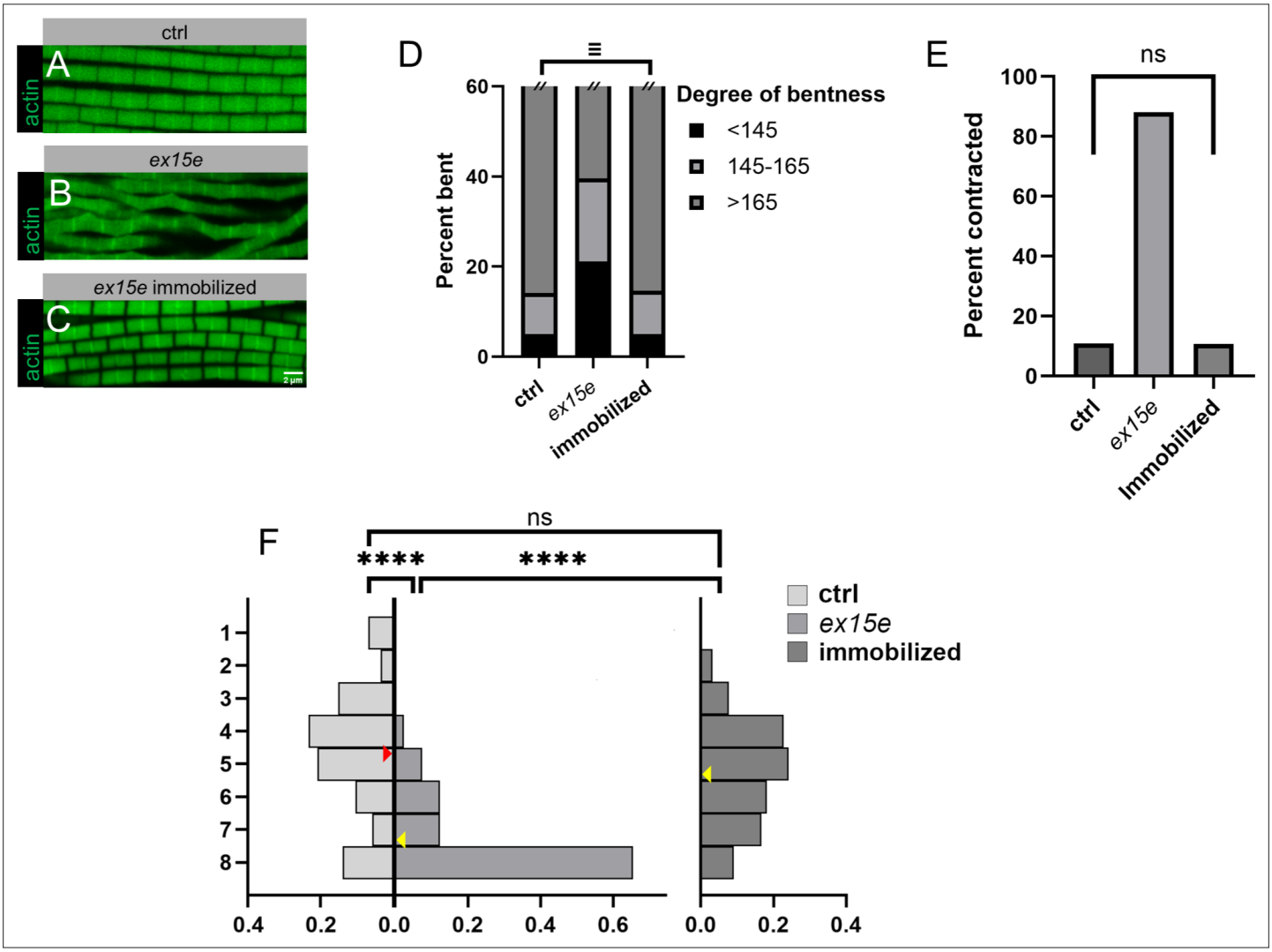

Figure 9. *ex15e* defects are rescued by immobilization. Rescues were attempted by immobilizing flies, thereby preventing indirect flight muscle (IFM) use. *ex15e* myofibrils in flies that were immobilized (**C**) resembled those of ctrl (**A**), both showing no phenotypes compared to *ex15e* (**B**). (**D**) Bend angles were equivalent between ctrl and *ex15e* immobilized flies (*n*=2119) (two one-sided test [TOST] with ±4.5° equivalence margin, α=0.05; t_L = 15.36, t_U = −12.00). (**E**) The proportion of sarcomeres that were contracted was not significantly different between ctrl and immobilized flies (*n*=2246) (Fisher's exact test; p=0.9037). (**F**) Flight ability was rescued with immobilized flies (*n*=67 flies) having no significant flight defect compared to ctrl (*n*=86) but being significantly improved from their non-immobilized counterparts (*n*=81) (Fisher's exact test; ctrl-immobilized p=0.0640; ctrl-*ex15e* and *ex15e*-immobilized p<0.0001).

Intriguingly, even flight ability was restored in immobilized flies compared to age-matched controls with no significant difference between the two (***Figure 9F***). These results suggest successful rescue by preventing IFM use via immobilization.

Discussion

Traditionally, IDRs were associated with the concept of amorphousness, finding themselves in transient structures such as condensates and membraneless organelles. As our understanding of disordered proteins has changed, their role in more disparate contexts has become increasingly appreciated, revealing them as modular hubs, flexible scaffolds, and more (***Cortese et al., 2008***). Furthermore, their role in disease has spurred great interest in their myriad functions. In this study, we demonstrate the role of an exceptionally large disordered region, Zasp52's exon 15e, in maintaining stability and integrity in a highly rigid and force-bearing structure – the Z-disc.

First, we showed that the expression of exon 15e is spatiotemporally regulated. Being confined to the adult IFM suggests that exon 15e's function is uniquely required for the rapid oscillatory contractions in indirect flight. Supporting this is the fact that the linker region containing exon 15e is generally much longer in Drosophilids and rather short in insects using direct flight. Although this linker region is predicted by multiple software programs to be disordered, within it are regions of greater order, one of which corresponds to a putative ABM (***Ashour et al., 2023***). This arrangement exists in other proteins such as Cno in *Drosophila*, where higher-ordered actin-binding regions are embedded in a large IDR (***Jensen et al., 2025***). Furthermore, a synthetic enhancement between *ex15e* and $Act88F^{KM88}$ heterozygotes indicates that exon 15e and actin genetically interact. There may be other important short linear motifs contained within the linker region, which serve as interacting sites with other sarcomere proteins. Indeed, multiple sequence alignment of the linker regions of various insects reveals several conserved motifs of unknown function. The presence of an ABM that may strengthen thin filament anchoring to the Z-disc would be in line with the phenotypes we observed in *ex15e*. However, we were unable to detect defects in our deletion of this motif, which supports the theory that the entire IDR is essential and that the ABM is not the key to its function. It is still possible that the ABM within exon 15e acts in concert with the N-terminal ABM, but specific amino acids mediating the N-terminal actin binding have not yet been identified (***Liao et al., 2020***). Bending at the Z-disc is indicative of a loss of thin filament anchoring and stability at the Z-disc, allowing them to shift out of alignment. Normal sarcomeres bent due to force would exhibit a kinked-hose appearance, where the inner edge is sharply bent and the outer one bowed. This was occasionally observed in controls, whereas *ex15e* bends were always shifted uniformly. Actin in the H-zone is also indicative of loss of stable thin filament anchoring. During preparation, IFMs are incubated overnight in skinning solution during which they enter a state of rigor. After washing them with an ATP-containing relaxing solution, the myosin heads detach from the thin filaments and the supple nature of the sarcomere, which provides it with elastic recoil, causes it to resume a relaxed conformation. However, when thin filaments are weakly anchored at the Z-discs, the natural tension contained within the sarcomere is reduced and thus it will not 'bounce back' into a relaxed conformation, resulting in a hypercontracted state which manifests as actin continuing to reside in the H-zone. Cheerio, a *Drosophila* filamin, was shown to stably attach actin thin filaments at the Z-disc and induces a similar actin incorporation into the H-zone when mutated (***González-Morales et al., 2017***). Thus, we also demonstrate the importance of Z-disc integrity in allowing sarcomeres to return to their relaxed state in rapidly contracting asynchronous IFM. Accordingly, synchronous muscles do not have such regularly structured Z-discs and do not require Zasp52's exon 15e. Indeed, exon 15e is absent in larval and other muscle types. We therefore propose that exon 15e is uniquely required to stabilize rapidly contracting asynchronous IFM.

The orthologous human ALP/Enigma family consists of seven members, with LDB3 (ZASP) considered the canonical Zasp52 ortholog. Zasp52 is more precisely a combined ALP/Enigma member; its first LIM domain is sequentially homologous to the single LIM domain of human ALP family members, and its last three LIM domains are homologous to the three Enigma family LIM domains. Though these human proteins do contain disordered linkers connecting their structured domains, they are much shorter than in *Drosophila* and are not sequentially homologous. The length of *Drosophila*'s linker was likely evolutionarily driven to be large, as we see insects using direct flight to have much shorter linkers. Several pathological mutations have been identified in the linker region between LDB3's PDZ

and LIM domains (***Vatta et al., 2003***), some of which are now known to lie in the actin-binding ZM (***Lin et al., 2014***), which corresponds to the actin-binding region N-terminal to Zasp52 LIM1 (***Liao et al., 2020***). Interestingly, LDB3 has three skeletal muscle-specific splice isoforms, which are differentially expressed and variably retain/omit exons 9 through 11 of a linker sequence (***Lin et al., 2014***). The prenatal long (L) isoform contains exons 10 and 11, post-natal long (LΔex10) has only exon 11, and short (S) has only 9. Post-natal LDB3-LΔex10 contains an actin-binding region in its linker region whose function is abolished by the inclusion of exon 10 in LDB3-L. Thus, human Zasp protein linkers also function in actin binding, regulated by developmentally differential expression. Linker regions in several human ALP/Enigma proteins were found to interact with both α-actinin and actin using AlphaFold (***Healy and Collins, 2023***). The mouse ortholog Cypher also contains tissue-specific splice variants which variably include or omit linker sequences (***Huang et al., 2003***). Like Zasp52's exon 15e, Cypher is not required for sarcomerogenesis or Z-disc assembly but only maintenance (***Zhou et al., 2001***).

Our genetic rescues support our hypothesis of exon 15e involvement in stabilizing thin filaments and Z-discs. The rescues also demonstrate that the conserved domains (PDZ, ZM, LIM1-4) are not sufficient for proper Z-disc and thin filament stability in IFM, because Zasp52-PR could not rescue any of the defects. Interestingly, these phenotypes, as well as the flight defects we observed, worsened with age, with defects in 1-day-old flies being very minor. This implies that exon 15e is not required developmentally, but rather for the maintenance of sarcomeres which naturally deteriorate with use. We originally hypothesized that since IDRs often lead to protein aggregation and phase separation, exon 15e might drive the formation of Z-bodies, primitive Z-discs which form through the coalescence of diffuse Z-disc proteins, including Zasp52. However, given the lack of defects in early Z-discs and the fact that exon 15e expression does not temporally coincide with Z-body formation, we reject this hypothesis. The role of exon 15e in maintenance is supported by immobilization rescues, in which flies were prevented from flying. We opted for a low-ceiling apparatus which we believe would not only prevent flies from flying but discourage them from futilely attempting to utilize their IFM at all. Surprisingly, immobilization restored flight ability to wild-type levels. Interestingly, human zaspopathies often manifest late in life, with one study citing onset at 44–73 years of age (***Selcen and Engel, 2005***), much like what we observed in flies. Our data suggest that avoiding strenuous exercise might delay the onset of zaspopathies. Given the maintenance-specific role of exon 15e, but also that as a whole, Zasp52 is indispensable for pupal myofibril development and not just maintenance (***Katzemich et al., 2013***; ***Medina-Quintana et al., 2026***), Zasp52 appears to have a multifaceted role more complex than previously considered.

It was demonstrated in ***Liao et al., 2016***, that various structured domains of Zasp52, such as the C-terminal LIM domains, are sufficient to localize to the Z-disc. We found that the disordered exon 15e was also able to localize to the Z-disc, indicating that some feature contained within it is capable of targeting the protein to its correct location. We took advantage of this to assess its kinetics using FRAP and found that the exon 15e construct is much less dynamic than Zasp52-PR (which lacks exon 15e), suggesting that this disordered region is important for anchoring the protein in place. This finding supports the theory that the IDR acts to stabilize thin filaments at the Z-disc. Although 1-day-old *ex15e* myofibrils are morphologically indistinguishable from controls, we were already able to detect abnormalities in Zasp52 dynamics using FRAP in our mutant background. The presence of recovery suggests that certain Zasp52 isoforms are not immobile as might be assumed for an anchoring protein and do indeed possess kinetics on a sub-minute timeframe. This is supported by significant transcription of the gene, including exon 15e-containing isoforms, into adulthood. The mobile fraction of Zasp52-PR was significantly increased in a system entirely lacking exon 15e (the PR isoform also lacks exon 15e), indicating a role of exon 15e in retaining Zasp52 at the Z-disc, whether by direct interaction or not. The FRAP data suggest that Zasp52's IDR stabilizes the Z-disc, in line with the electron microscopy data. It suggests that Z-discs can be described as highly solid aggregates in part stabilized by IDRs, on the other end of the spectrum of the transient condensates initially described, thereby further expanding the importance of IDRs for establishing subcellular structures.

Overall, Zasp52 and its isoforms represent a complex toolbox of multifunctional proteins. There has been evidence suggesting that Zasp52 is not required for initial sarcomere assembly in embryos (***Rui et al., 2010***), important for Z-disc maintenance overall (***Rui et al., 2010***; ***Jani and Schöck, 2007***; ***Katzemich et al., 2013***), and required for pupal myofibril assembly (***Katzemich et al., 2013***). The complete picture of Zasp52's varied function is still unclear; however, we have shown that a specific

disordered region is required for maintaining IFM and stabilizing the rigidity of Z-discs. The long linker might not only contain protein-interacting regions and provide the glue to hold the Z-disc together but might also provide the spacing needed for the neighboring structured domains to properly interact with their partners and perform their roles. We have seen in our genetic interaction experiment an inability of thin filaments to properly elongate when Act88F is partially depleted, which further implicates exon 15e not only in Act88F structure but dynamics. Most encouraging is the complete rescue of flight ability through immobilization, which may provide avenues for delaying the onset of human zaspopathies through reducing strenuous exercise.

Materials and methods

Key resources table

Reagent type (species) or resource	Designation	Source or reference	Identifiers	Additional information
Gene (*Drosophila melanogaster*)	Zasp52	FlyBase	FBgn0265991	
Gene (*Drosophila melanogaster*)	Act88F	FlyBase	FBgn0000047	
Strain, strain background (*D. melanogaster*)	*ex15e*	This paper		See Materials and methods – Fly strains and husbandry
Strain, strain background (*D. melanogaster*)	*Zasp52^{MI00979}*	BDSC	RRID:BDSC_33099	
Strain, strain background (*D. melanogaster*)	*Df(2R)BSC427*	BDSC	RRID:BDSC_24931	
Strain, strain background (*D. melanogaster*)	*ΔABM*	This paper		See Materials and methods – Fly strains and husbandry
Strain, strain background (*D. melanogaster*)	UAS-Zasp52-PF	This paper		See Materials and methods – Fly strains and husbandry
Strain, strain background (*D. melanogaster*)	UAS-Zasp52-PR	This paper		See Materials and methods – Fly strains and husbandry
Strain, strain background (*D. melanogaster*)	UH3-GAL4	***Singh et al., 2014***	FBti0148868	
Strain, strain background (*D. melanogaster*)	*Act88F^{KM88}*	FlyBase	FBal0000272	
Strain, strain background (*D. melanogaster*)	UAS-GFPexon15e	This paper		See Materials and methods – Fly strains and husbandry
Strain, strain background (*D. melanogaster*)	UAS-GFPZasp52-PR	***González-Morales et al., 2019***	FBtp0140762	
Strain, strain background (*D. melanogaster*)	*w^{1118}*	FlyBase	FBal0018186	
Antibody	Anti-Zasp52 full-length (Rabbit polyclonal)	***Jani and Schöck, 2007***		1:200
Antibody	Anti-Zasp52LIM234 (Rabbit polyclonal)	This paper		See Materials and methods – Western blotting
Antibody	Anti-βPS integrin (Mouse monoclonal)	DSHB	CF.6G11	1:200
Antibody	Goat anti-rabbit IgG (H+L) HRP	Thermo Fisher Scientific	Cat 31460	1:10000
Antibody	Alexa Fluor 647 goat anti-rat	Thermo Fisher Scientific	Cat A-21247	1:400
Antibody	Alexa Fluor 488 goat anti-rabbit	Thermo Fisher Scientific	Cat A-11008	1:400
Antibody	Acti-stain 555 fluorescent phalloidin	Cytoskeleton Inc	Cat PHDH1	1:400
Antibody	FluoTag-X4 anti-GFP	NanoTag Biotechnologies	Cat N0304	1:200

Continued on next page

Continued

Reagent type (species) or resource	Designation	Source or reference	Identifiers	Additional information
Software, algorithm	IBS 2.0	***Xie et al., 2022***		
Software, algorithm	SMART	***Letunic and Bork, 2018***		
Software, algorithm	Salmon 1.10.0	***Patro et al., 2017***		
Software, algorithm	AIUPred v0.1	***Erdős and Dosztányi, 2024***		
Software, algorithm	DISOPRED3	***Jones and Cozzetto, 2015***		
Software, algorithm	metapredict online v3.0	***Emenecker et al., 2021***		
Software, algorithm	AlphaFold v2.0	***Jumper et al., 2021***		
Software, algorithm	iTOL v.6	***Letunic and Bork, 2024***		
Software, algorithm	NARDINI	***Cohan et al., 2022***		

Fly strains and husbandry

Flies were housed at room temperature (22°C) in standard glass vials and food unless indicated otherwise. Immobilized flies were reared in between 3.25×3.25 inch glass plates separated by 1.5 mm spacers; standard food was inserted into the gap. Immobilized flies were transferred to a new apparatus with fresh food every couple of days. *ex15e* flies were created by Genetivision using CRISPR-mediated homology-directed repair. The gRNA sequences used were TTTGAACTTGAACTCTAATG TGG for the downstream target and CAGCCTCTCCACCTTTCCGATGG for upstream. The deletion was replaced with a cassette containing a 3xP3DsRed marker flanked by attP landing sites. It was validated by sequencing at the cut sites. *ΔABM* flies were created by Genome ProLab using CRISPR-mediated homology-directed repair as well. The gRNA sequence GAGGAGCTCTCGGGTCTGCA was used to precisely delete five amino acids (LQREL), verified by sequencing. The following genotypes were used: *ex15e*, *ΔABM*, w^{1118} as control in all experiments, *Df(2R)BSC427*, $Act88F^{KM88}$, UAS-GFPZasp52-PR, UH3-Gal4, UAS-Zasp52-PF, UAS-Zasp52-PR, UAS-GFPexon15e, and $Zasp52^{MI00979}$. UAS-Zasp52-PF and UAS-Zasp52-PR consist of the respective Zasp52 isoform plus an N-terminal ALFA-tag and C-terminal Spot tag. UAS-GFPexon15e encompasses all amino acids encoded by exon 15e except the last nine encoding the beginning of LIM2. All UAS constructs were made by Genscript and injected into w^{1118} by GenomeProlab.

Western blotting

Extracts were prepared by homogenizing 10 flies/fly parts in 100 µL RIPA buffer with protease inhibitor plus an equal amount of 2× Laemmli buffer with β-mercaptoethanol. Samples were boiled at 95°C for 5 min and centrifuged at 12,000×rcf for 5 min. Supernatant was used for electrophoresis according to standard protocol using a 4–15% Bio-Rad TGX Stain-free gel. Stain-free gels were imaged for total protein content on a Bio-Rad ChemiDoc before protein was transferred onto a nitrocellulose membrane. Standard western blotting procedures were followed. Primary antibodies used were rabbit anti-Zasp52 full-length (***Jani and Schöck, 2007***) and a rabbit antibody against the three C-terminal LIM domains of Zasp52 (FEKYLAPTCSKCAGKIKGDCLNAIGKHFHPECFTCGQCGKIFGNRPFF LEDGN AYCEADWNELFTTKCFACGFPVEAGDRWVEALNHNYHSQCFNCTFCKQNLEGQSFYNKGG RPFCKNHAR) made by Genscript; secondary antibody was goat anti-rabbit IgG (H+L) HRP (Thermo Fisher Scientific).

Locomotory assays

For flight assays, flies were reared in vials (unless immobilized) until the desired age, with vials flipped whenever pupae began to appear. Flight assays were conducted in a manner similar to that described in ***Babcock and Ganetzky, 2014***. A tube 22 cm long and 3.2 cm in diameter was placed in a funnel; the bottom of the tube rested 4 cm above the bottom spout of the funnel. The funnel rested in a 60 cm long tube, which was 13.5 cm in diameter and covered with TAD Shake & Spray glue (LADD

Research) on the inside. The bottom of the funnel was 12 cm below the top of the larger tube. The larger tube was divided vertically into seven 8.5 cm segments, with segment 1 being at the top, and segment 7 being at the bottom. A dish containing water was placed below the tube and was considered segment 8. Vials containing flies were dropped down the narrow tube so that they would be ejected into the larger tube and land somewhere along its length. Flies naturally fly upward and those with stronger flight would land higher up the tube. Binary flight assays were conducted by releasing flies one at a time and recording whether they could generate any upward lift. They were raised in the same conditions as above.

For larval crawling assays, third instar larvae of the desired genotype were collected from bottles and assayed according to ***Post and Paululat, 2018***. In brief, videos of larvae on a slightly moistened Petri dish were taken. Time segments where larvae were crawling in a straight line continuously for at least 10 s were analyzed – contractions per distance were measured and recorded.

Muscle preparation and immunofluorescence

Primary antibodies used were rabbit anti-Zasp52 full-length (***Jani and Schöck, 2007***) and mouse anti-βPS-integrin (CF.6G11; obtained from Developmental Studies Hybridoma Bank, ***Brower et al., 1984***) at a concentration of 1:200 for both. Secondary antibodies used were Alexa Fluor 647 goat anti-rat (Thermo Fisher Scientific) and Alexa Fluor 488 goat anti-rabbit (Thermo Fisher Scientific) at a concentration of 1:400.

For IFM tissue, a protocol similar to ***Xiao et al., 2017***, was followed (refer to for recipes). Briefly, thoraces were bisected and incubated in Relaxing-Glycerol solution at –20°C overnight. IFMs were isolated and fixed in 4% paraformaldehyde for 15 min. Fixed IFMs were incubated in primary antibodies at 4°C overnight. IFMs were incubated in Acti-stain 555 fluorescent phalloidin (Cytoskeleton Inc) and secondary antibodies, at room temperature for 1 hr. Samples were mounted in Mowiol mounting medium.

For thorax hemisections, including MTZ, a scalpel was used to sagittally bisect thoraces. Samples were fixed in 4% paraformaldehyde for 15 min and incubated in primary antibodies for 1 hr at room temperature, and then Acti-stain 555 fluorescent phalloidin and secondary antibodies for 1 hr at room temperature. Samples were mounted in Mowiol mounting medium using three 0.12 mm spacers.

For TEM, bisected thoraces were treated with 5 mM MOPS, 150 mM KCl, 5 mM EGTA, 5 mM $MgCl_2$, 5 mM ATP, 1% Triton X-100, and protease inhibitor for 2 hr, then the same solution with 50% glycerol instead of Triton X-100 overnight at 4°C. This was repeated at –20°C. Samples were washed in 5 mM MOPS, 40 mM KCl, 5 mM EGTA, 5 mM $MgCl_2$, 5 mM NaN_3, protease inhibitor, and then fixed in 3% glutaraldehyde and 0.2% tannic acid for 2 hr. Samples were washed in 20 mM MOPS, 5 mM EGTA, 5 mM $MgCl_2$, 5 mM NaN_3, and then in 100 mM sodium phosphate buffer, 5 mM $MgCl_2$, 5 mM NaN_3. Secondary fixation was performed in 1% osmium tetroxide in the previous sodium phosphate buffer for 1 hr. Samples were stained in 2% uranyl acetate, washed with water, and underwent a serial dehydration in ethanol. Samples were washed with propylene oxide and serially infiltrated with Mollenhauer Epon-Araldite. After curing in Beem capsules, 70 nm sections were cut and stained in 4% uranyl acetate followed by SATO lead stain.

Fluorescence recovery after photobleaching

The sequence encoding exon 15e minus the nine C-terminal amino acids encoding LIM2 was subcloned into pUAST-attB-GFP-V5-His and injected into w^{1118}. IFM were prepared as previously described (with fixation) and stained with ActiStain-555 and FluoTag-X4 anti-GFP (NanoTag Biotechnologies) to visualize localization; FRAP was performed as described below. One-day-old female flies were anesthetized and their abdomens, wings, and legs removed. Carcasses were pinned down by the head on a silicone dish and immersed in hemolymph-like 3 (HL3) saline (***Stewart et al., 1994***). Thoraces were sagittally bisected, washed thrice in HL3 saline, and mounted with a 0.12 mm spacer. Imaging was performed immediately using an HC PL APO 63×/1.40 OIL CS2 objective on a Leica SP8 point-scanning confocal microscope. Five pre-bleach frames (1.29 s each) were recorded before bleaching with a 488 nm laser to achieve a bleach depth averaging 75% ± 4% (SD) for UH3>GFPexon15e, 74% ± 8% for UH3>GFPZasp52-PR, 77% ± 7% for *ex15e*; UH3>GFPZasp52-PR, and 76% ± 9% for fixed samples. Seventy-five post-bleach frames (1.29 s each) were then acquired. ROIs (1.25×3 µm) were placed over individual Z-discs and those with drift were discarded. For each fly, three Z-discs on different myofibrils were

bleached, and intensities of adjacent unbleached Z-discs and unbleached background regions were recorded. Fluorescence was normalized as (bleached–background)/(unbleached–background), averaged across the three ROIs, and scaled such that the post-bleach frame equaled 0 and the pre-bleach mean equaled 100. Recovery curves were presented as mean ± SEM. Each fly's curve was fitted to a one-phase exponential association model to obtain the plateau (mobile fraction). Fixed UH3>GFP-Zasp52-PR samples were prepared in the same manner except with an additional 10 min fixation in 4% paraformaldehyde in HL3 saline.

Microscopy

Confocal images were acquired using an HC PL APO 63×/1.40 OIL CS2 objective on a Leica SP8 point-scanning confocal microscope. The position along the z-axis was adjusted until perfectly in the center of the myofibril, i.e., the widest point. Polarized light images were acquired using a 5× N-ACHROPLAN, NA = 0.13 objective on a Zeiss Axio Observer microscope. TEM images were acquired using an FEI Tecnai G2 Spirit Twin 120 kV Cryo-TEM using an AMT NanoSprint15 MK2 CMOS camera.

Computational analyses

Schematics were illustrated with IBS 2.0 (***Xie et al., 2022***). All protein domains were defined per SMART (***Letunic and Bork, 2018***). Graphing and statistical analysis were performed using GraphPad Prism 10. Statistical analyses were performed in GraphPad Prism 10, where ns = $p \geq 0.05$, *=$p<0.05$; **=$p<0.01$, and ****=$p<0.0001$, and calculated to four decimal places. Equivalence of bend angles was assessed using the two one-sided test (TOST) procedure. Model sarcomeres with bend angles ranging from 180° (straight) to 95° and blurring were generated. Each was hand-measured 10 times, and the average absolute measurement error (4.5°) was used as the equivalence margin for all TOST analyses.

Minus strand RNA-seq bigWig files from the ENCODE project (***Duff et al., 2015***) with the following accessions were retrieved and loaded in IGV 2.19.4 (***Robinson et al., 2011***): ENCFF289ZZT, ENCFF982OGI, ENCFF430HWM, ENCFF716DNU, ENCFF829OGQ, ENCFF936YJM, ENCFF987YVI, ENCFF033MIY, ENCFF845HII, ENCFF021VXY, ENCFF792FNT. Signal tracks were aligned to the dm3 assembly, and the data range was adjusted uniformly for all tracks.

SRA files with the following accession numbers were downloaded from the Bioproject PRJNA419412 (***Spletter et al., 2018***): SRR6314253, SRR6314256, SRR6314275, SRR6314259, SRR6314277, SRR6314262, SRR6314273. Salmon 1.10.0 (***Patro et al., 2017***) was used to quantify expression of the following transcripts which correspond to identified Zasp52 isoforms: FBtr0392902, FBtr0329914, FBtr0329912, FBtr0100387, FBtr0111048, FBtr0087315, FBtr0329913, FBtr0310086, FBtr0329916, FBtr0329915, FBtr0310088, FBtr0310087, FBtr0392901, FBtr0329911, FBtr0342711, FBtr0100388, FBtr0302163, FBtr0301313, FBtr0479884, FBtr0329909, FBtr0392918, FBtr0329910. The first six were classified as containing only exon 15a, the next six containing exons 15b–d, the next four containing exon 15e, and the last six containing no exon 15.

ImageJ was used to evaluate bending manually using the angle tool, and sarcomere length using the line measuring tool.

For disorder prediction, the entire Zasp52-PF sequence was entered into AIUPred v0.1 (***Erdős and Dosztányi, 2024***), DISOPRED3 (***Jones and Cozzetto, 2015***) (as two sequences, the first covering the first 1200 amino acids and the second, the remaining), or metapredict online v3.0 (***Emenecker et al., 2021***). Raw values for each residue were obtained and smoothed using a Savitzky-Golay filter with fourth order smoothing and 11 neighbors on each side. AlphaFold v2.0 (***Jumper et al., 2021***) was used to obtain pLDDT scores for the alpha carbon of each residue. pLDDT scores were min-max normalized and smoothed in the same manner as above.

Zasp52 orthologs were obtained for members of the class *Insecta* using NCBI's Eukaryotic Genome Annotation Pipeline. Canonical protein sequences for each were downloaded and those which did not contain the classical PDZ and four LIM domains were removed. The number of residues between the first and second LIM domains was calculated. A phylogenetic tree of these species was created using NCBI's Common Tree (***Schoch et al., 2020***) and a heatmap created using iTOL v.6 (***Letunic and Bork, 2024***).

NARDINI (***Cohan et al., 2022***) was used for the sequences indicated to generate a z-score matrix, with 100,000 scrambled sequence variants.

Acknowledgements

This work was funded by the Canadian Institutes of Health Research project grant PJT-178114. Confocal images were collected in the McGill University Advanced Bioimaging Facility (ABIF). Electron microscopy images were collected and analyzed in the McGill University Facility for Electron Microscopy Research (FEMR).

Additional information

Funding

Funder	Grant reference number	Author
Canadian Institutes of Health Research	project grant PJT-178114	Frieder Schöck

The funders had no role in study design, data collection and interpretation, or the decision to submit the work for publication.

Author contributions

Nikolai Ho, Conceptualization, Data curation, Software, Formal analysis, Validation, Investigation, Visualization, Methodology, Writing - original draft, Writing – review and editing; Frieder Schöck, Conceptualization, Supervision, Funding acquisition, Validation, Project administration, Writing – review and editing

Author ORCIDs

Nikolai Ho https://orcid.org/0009-0001-6027-7824
Frieder Schöck https://orcid.org/0000-0002-1351-0574

Peer review material

Version of Record:
Reviewer #1 (Public review): https://doi.org/10.7554/eLife.111101.3.sa1
Reviewer #2 (Public review): https://doi.org/10.7554/eLife.111101.3.sa2
Author response https://doi.org/10.7554/eLife.111101.3.sa3

Reviewed preprint v2
Reviewer #1 (Public review): https://doi.org/10.7554/eLife.111101.2.sa2
Reviewer #2 (Public review): https://doi.org/10.7554/eLife.111101.2.sa1
Author response: https://doi.org/10.7554/eLife.111101.2.sa0
eLife Assessment https://doi.org/10.7554/eLife.111101.2.sa3

Reviewed preprint v1
Reviewer #1 (Public review): https://doi.org/10.7554/eLife.111101.1.sa2
Reviewer #2 (Public review): https://doi.org/10.7554/eLife.111101.1.sa1
Author response: https://doi.org/10.7554/eLife.111101.1.sa0
eLife Assessment https://doi.org/10.7554/eLife.111101.1.sa3

Additional files

Supplementary files

MDAR checklist

Data availability

All data generated or analyzed during this study is available on figshare: https://doi.org/10.6084/m9.figshare.32411457.v1, https://doi.org/10.6084/m9.figshare.32411487.v1, https://doi.org/10.6084/m9.figshare.32425929.v1, https://doi.org/10.6084/m9.figshare.32426091.v1, https://doi.org/10.6084/m9.figshare.32426178.v1, https://doi.org/10.6084/m9.figshare.32426268.v1, https://doi.org/

10.6084/m9.figshare.32426346.v1, https://doi.org/10.6084/m9.figshare.32915378.v1, https://doi.org/10.6084/m9.figshare.32915384.v1, https://doi.org/10.6084/m9.figshare.32915387.v1, https://doi.org/10.6084/m9.figshare.32915396.v1.

The following datasets were generated:

Author(s)	Year	Dataset title	Dataset URL	Database and Identifier
Nikolai H	2026	Figure 1 supplementary data	https://doi.org/10.6084/m9.figshare.32411457.v1	figshare, 10.6084/m9.figshare.32411457.v1
Nikolai H	2026	Figure 2 supplementary data	https://doi.org/10.6084/m9.figshare.32411487.v1	figshare, 10.6084/m9.figshare.32411487.v1
Nikolai H	2026	Figure 3 supplementary data	https://doi.org/10.6084/m9.figshare.32425929.v1	figshare, 10.6084/m9.figshare.32425929.v1
Nikolai H	2026	Figure 4 supplementary data	https://doi.org/10.6084/m9.figshare.32426091.v1	figshare, 10.6084/m9.figshare.32426091.v1
Nikolai H	2026	Figure 5 supplementary data	https://doi.org/10.6084/m9.figshare.32426178.v1	figshare, 10.6084/m9.figshare.32426178.v1
Nikolai H	2026	Figure 6 supplementary data	https://doi.org/10.6084/m9.figshare.32426268.v1	figshare, 10.6084/m9.figshare.32426268.v1
Nikolai H	2026	Figure 7 supplementary data	https://doi.org/10.6084/m9.figshare.32426346.v1	figshare, 10.6084/m9.figshare.32426346.v1
Nikolai H	2026	Figure 8 supplementary data	https://doi.org/10.6084/m9.figshare.32915378.v1	figshare, 10.6084/m9.figshare.32915378.v1
Nikolai H	2026	Figure 9 supplementary data	https://doi.org/10.6084/m9.figshare.32915384.v1	figshare, 10.6084/m9.figshare.32915384.v1
Nikolai H	2026	Figure S2 supplementary data	https://doi.org/10.6084/m9.figshare.32915387.v1	figshare, 10.6084/m9.figshare.32915387.v1
Nikolai H	2026	Figure S3 supplementary data	https://doi.org/10.6084/m9.figshare.32915396.v1	figshare, 10.6084/m9.figshare.32915396.v1

References

Ashour DJ, Durney CH, Planelles-Herrero VJ, Stevens TJ, Feng JJ, Röper K. 2023. Zasp52 strengthens whole embryo tissue integrity through supracellular actomyosin networks. *Development* **150**:dev201238. DOI: https://doi.org/10.1242/dev.201238, PMID: 36897564

Babcock DT, Ganetzky B. 2014. An improved method for accurate and rapid measurement of flight performance in *Drosophila*. *Journal of Visualized Experiments* **84**:e51223. DOI: https://doi.org/10.3791/51223, PMID: 24561810

Benna C, Peron S, Rizzo G, Faulkner G, Megighian A, Perini G, Tognon G, Valle G, Reggiani C, Costa R, Zordan MA. 2009. Post-transcriptional silencing of the *Drosophila* homolog of human ZASP: a molecular and functional analysis. *Cell and Tissue Research* **337**:463–476. DOI: https://doi.org/10.1007/s00441-009-0813-y, PMID: 19603185

Bothe I, Baylies MK. 2016. *Drosophila* myogenesis. *Current Biology* **26**:R786–R791. DOI: https://doi.org/10.1016/j.cub.2016.07.062, PMID: 27623256

Bouaouina M, Jani K, Long JY, Czerniecki S, Morse EM, Ellis SJ, Tanentzapf G, Schöck F, Calderwood DA. 2012. Zasp regulates integrin activation. *Journal of Cell Science* **125**:5647–5657. DOI: https://doi.org/10.1242/jcs.103291, PMID: 22992465

Brower DL, Wilcox M, Piovant M, Smith RJ, Reger LA. 1984. Related cell-surface antigens expressed with positional specificity in *Drosophila* imaginal discs. *PNAS* **81**:7485–7489. DOI: https://doi.org/10.1073/pnas.81.23.7485, PMID: 6390440

Chechenova MB, Bryantsev AL, Cripps RM. 2013. The Drosophila Z-disc protein Z(210) is an adult muscle isoform of Zasp52, which is required for normal myofibril organization in indirect flight muscles. *The Journal of Biological Chemistry* **288**:3718–3726. DOI: https://doi.org/10.1074/jbc.M112.401794, PMID: 23271733

Cohan MC, Shinn MK, Lalmansingh JM, Pappu RV. 2022. Uncovering non-random binary patterns within sequences of intrinsically disordered proteins. *Journal of Molecular Biology* **434**:167373. DOI: https://doi.org/10.1016/j.jmb.2021.167373, PMID: 34863777

Cortese MS, Uversky VN, Dunker AK. 2008. Intrinsic disorder in scaffold proteins: getting more from less. *Progress in Biophysics and Molecular Biology* **98**:85–106. DOI: https://doi.org/10.1016/j.pbiomolbio.2008.05.007, PMID: 18619997

Duff MO, Olson S, Wei X, Garrett SC, Osman A, Bolisetty M, Plocik A, Celniker SE, Graveley BR. 2015. Genome-wide identification of zero nucleotide recursive splicing in Drosophila. *Nature* **521**:376–379. DOI: https://doi.org/10.1038/nature14475, PMID: 25970244

Emenecker RJ, Griffith D, Holehouse AS. 2021. Metapredict: a fast, accurate, and easy-to-use predictor of consensus disorder and structure. *Biophysical Journal* **120**:4312–4319. DOI: https://doi.org/10.1016/j.bpj.2021.08.039, PMID: 34480923

Erdős G, Dosztányi Z. 2024. AIUPred: combining energy estimation with deep learning for the enhanced prediction of protein disorder. *Nucleic Acids Research* **52**:W176–W181. DOI: https://doi.org/10.1093/nar/gkae385, PMID: 38747347

Fisher LAB, Schöck F. 2022. The unexpected versatility of ALP/Enigma family proteins. *Frontiers in Cell and Developmental Biology* **10**:963608. DOI: https://doi.org/10.3389/fcell.2022.963608, PMID: 36531944

González-Morales N, Holenka TK, Schöck F. 2017. Filamin actin-binding and titin-binding fulfill distinct functions in Z-disc cohesion. *PLOS Genetics* **13**:e1006880. DOI: https://doi.org/10.1371/journal.pgen.1006880, PMID: 28732005

González-Morales N, Xiao YS, Schilling MA, Marescal O, Liao KA, Schöck F. 2019. Myofibril diameter is set by a finely tuned mechanism of protein oligomerization in *Drosophila eLife* **8**:e50496. DOI: https://doi.org/10.7554/eLife.50496, PMID: 31746737

Griggs R, Vihola A, Hackman P, Talvinen K, Haravuori H, Faulkner G, Eymard B, Richard I, Selcen D, Engel A, Carpen O, Udd B. 2007. Zaspopathy in a large classic late-onset distal myopathy family. *Brain* **130**:1477–1484. DOI: https://doi.org/10.1093/brain/awm006, PMID: 17337483

Healy MD, Collins BM. 2023. The PDLIM family of actin-associated proteins and their emerging role in membrane trafficking. *Biochemical Society Transactions* **51**:2005–2016. DOI: https://doi.org/10.1042/BST20220804, PMID: 38095060

Huang C, Zhou Q, Liang P, Hollander MS, Sheikh F, Li X, Greaser M, Shelton GD, Evans S, Chen J. 2003. Characterization and in vivo functional analysis of splice variants of cypher. *The Journal of Biological Chemistry* **278**:7360–7365. DOI: https://doi.org/10.1074/jbc.M211875200, PMID: 12499364

Jani K, Schöck F. 2007. Zasp is required for the assembly of functional integrin adhesion sites. *The Journal of Cell Biology* **179**:1583–1597. DOI: https://doi.org/10.1083/jcb.200707045, PMID: 18166658

Jensen CC, Gurley NJ, Mathias AJ, Wolfsberg LR, Xiao Y, Zhou Z, Bischoff MC, Clark SE, Slep KC, Peifer M. 2025. A key role of Canoe's intrinsically disordered region in linking cell junctions to the cytoskeleton. *The Journal of Cell Biology* **224**:e202505135. DOI: https://doi.org/10.1083/jcb.202505135, PMID: 41099653

Jones DT, Cozzetto D. 2015. DISOPRED3: precise disordered region predictions with annotated protein-binding activity. *Bioinformatics* **31**:857–863. DOI: https://doi.org/10.1093/bioinformatics/btu744, PMID: 25391399

Jumper J, Evans R, Pritzel A, Green T, Figurnov M, Ronneberger O, Tunyasuvunakool K, Bates R, Žídek A, Potapenko A, Bridgland A, Meyer C, Kohl SAA, Ballard AJ, Cowie A, Romera-Paredes B, Nikolov S, Jain R, Adler J, Back T, et al. 2021. Highly accurate protein structure prediction with AlphaFold. *Nature* **596**:583–589. DOI: https://doi.org/10.1038/s41586-021-03819-2, PMID: 34265844

Katzemich A, Long JY, Jani K, Lee BR, Schöck F. 2011. Muscle type-specific expression of Zasp52 isoforms in *Drosophila*. *Gene Expression Patterns* **11**:484–490. DOI: https://doi.org/10.1016/j.gep.2011.08.004, PMID: 21867777

Katzemich A, Liao KA, Czerniecki S, Schöck F. 2013. Alp/Enigma family proteins cooperate in Z-disc formation and myofibril assembly. *PLOS Genetics* **9**:e1003342. DOI: https://doi.org/10.1371/journal.pgen.1003342, PMID: 23505387

Krans JL. 2010. The sliding filament theory of muscle contraction. *Nature Education* **3**:66.

Letunic I, Bork P. 2018. 20 years of the SMART protein domain annotation resource. *Nucleic Acids Research* **46**:D493–D496. DOI: https://doi.org/10.1093/nar/gkx922, PMID: 29040681

Letunic I, Bork P. 2024. Interactive Tree of Life (iTOL) v6: recent updates to the phylogenetic tree display and annotation tool. *Nucleic Acids Research* **52**:W78–W82. DOI: https://doi.org/10.1093/nar/gkae268, PMID: 38613393

Liao KA, González-Morales N, Schöck F. 2016. Zasp52, a Core Z-disc Protein in *Drosophila* indirect flight muscles, interacts with α-actinin via an extended PDZ domain. *PLOS Genetics* **12**:e1006400. DOI: https://doi.org/10.1371/journal.pgen.1006400, PMID: 27783625

Liao KA, González-Morales N, Schöck F. 2020. Characterizing the actin-binding ability of Zasp52 and its contribution to myofibril assembly. *PLOS ONE* **15**:e0232137. DOI: https://doi.org/10.1371/journal.pone.0232137, PMID: 32614896

Lin X, Ruiz J, Bajraktari I, Ohman R, Banerjee S, Gribble K, Kaufman JD, Wingfield PT, Griggs RC, Fischbeck KH, Mankodi A. 2014. Z-disc-associated, alternatively spliced, PDZ motif-containing protein (ZASP) mutations in the

actin-binding domain cause disruption of skeletal muscle actin filaments in myofibrillar myopathy. *The Journal of Biological Chemistry* **289**:13615–13626. DOI: https://doi.org/10.1074/jbc.M114.550418, PMID: 24668811

Medina-Quintana J, Akbari-Gakieh B, Lalonde M-P, Liu T, Schöck F. 2026. Zasp52 in *Drosophila melanogaster* indirect flight muscles can serve as a model system to investigate the function of clinical variants causing myopathies. *G3* **16**:jkag148. DOI: https://doi.org/10.1093/g3journal/jkag148, PMID: 42262929

Nikonova E, Kao SY, Spletter ML. 2020. Contributions of alternative splicing to muscle type development and function. *Seminars in Cell & Developmental Biology* **104**:65–80. DOI: https://doi.org/10.1016/j.semcdb.2020.02.003, PMID: 32070639

Patro R, Duggal G, Love MI, Irizarry RA, Kingsford C. 2017. Salmon provides fast and bias-aware quantification of transcript expression. *Nature Methods* **14**:417–419. DOI: https://doi.org/10.1038/nmeth.4197, PMID: 28263959

Post Y, Paululat A. 2018. Muscle function assessment using a *Drosophila* larvae crawling assay. *BIO-PROTOCOL* **8**:e2933. DOI: https://doi.org/10.21769/BioProtoc.2933, PMID: 34395754

Robinson JT, Thorvaldsdóttir H, Winckler W, Guttman M, Lander ES, Getz G, Mesirov JP. 2011. Integrative genomics viewer. *Nature Biotechnology* **29**:24–26. DOI: https://doi.org/10.1038/nbt.1754, PMID: 21221095

Ruff KM, Pappu RV. 2021. AlphaFold and implications for intrinsically disordered proteins. *Journal of Molecular Biology* **433**:167208. DOI: https://doi.org/10.1016/j.jmb.2021.167208, PMID: 34418423

Rui Y, Bai J, Perrimon N. 2010. Sarcomere formation occurs by the assembly of multiple latent protein complexes. *PLOS Genetics* **6**:e1001208. DOI: https://doi.org/10.1371/journal.pgen.1001208, PMID: 21124995

Schoch CL, Ciufo S, Domrachev M, Hotton CL, Kannan S, Khovanskaya R, Leipe D, Mcveigh R, O'Neill K, Robbertse B, Sharma S, Soussov V, Sullivan JP, Sun L, Turner S, Karsch-Mizrachi I. 2020. NCBI Taxonomy: a comprehensive update on curation, resources and tools. *Database* **2020**:baaa062. DOI: https://doi.org/10.1093/database/baaa062, PMID: 32761142

Selcen D, Engel AG. 2005. Mutations in ZASP define a novel form of muscular dystrophy in humans. *Annals of Neurology* **57**:269–276. DOI: https://doi.org/10.1002/ana.20376, PMID: 15668942

Singh SH, Kumar P, Ramachandra NB, Nongthomba U. 2014. Roles of the troponin isoforms during indirect flight muscle development in *Drosophila*. *Journal of Genetics* **93**:379–388. DOI: https://doi.org/10.1007/s12041-014-0386-8, PMID: 25189233

Spletter ML, Barz C, Yeroslaviz A, Zhang X, Lemke SB, Bonnard A, Brunner E, Cardone G, Basler K, Habermann BH, Schnorrer F. 2018. A transcriptomics resource reveals a transcriptional transition during ordered sarcomere morphogenesis in flight muscle. *eLife* **7**:e34058. DOI: https://doi.org/10.7554/eLife.34058, PMID: 29846170

Steinmetz PRH, Kraus JEM, Larroux C, Hammel JU, Amon-Hassenzahl A, Houliston E, Wörheide G, Nickel M, Degnan BM, Technau U. 2012. Independent evolution of striated muscles in cnidarians and bilaterians. *Nature* **487**:231–234. DOI: https://doi.org/10.1038/nature11180, PMID: 22763458

Stewart BA, Atwood HL, Renger JJ, Wang J, Wu CF. 1994. Improved stability of Drosophila larval neuromuscular preparations in haemolymph-like physiological solutions. *Journal of Comparative Physiology A* **175**:179–191. DOI: https://doi.org/10.1007/BF00215114, PMID: 8071894

Vatta M, Mohapatra B, Jimenez S, Sanchez X, Faulkner G, Perles Z, Sinagra G, Lin JH, Vu TM, Zhou Q, Bowles KR, Di Lenarda A, Schimmenti L, Fox M, Chrisco MA, Murphy RT, McKenna W, Elliott P, Bowles NE, Chen J, et al. 2003. Mutations in Cypher/ZASP in patients with dilated cardiomyopathy and left ventricular non-compaction. *Journal of the American College of Cardiology* **42**:2014–2027. DOI: https://doi.org/10.1016/j.jacc.2003.10.021, PMID: 14662268

Venken KJT, Schulze KL, Haelterman NA, Pan H, He Y, Evans-Holm M, Carlson JW, Levis RW, Spradling AC, Hoskins RA, Bellen HJ. 2011. MiMIC: a highly versatile transposon insertion resource for engineering *Drosophila melanogaster* genes. *Nature Methods* **8**:737–743. DOI: https://doi.org/10.1038/nmeth.1662, PMID: 21985007

Watts NR, Zhuang X, Kaufman JD, Palmer IW, Dearborn AD, Coscia S, Blech-Hermoni Y, Alfano C, Pastore A, Mankodi A, Wingfield PT. 2017. Expression and Purification of ZASP subdomains and clinically important isoforms: high-affinity binding to G-Actin. *Biochemistry* **56**:2061–2070. DOI: https://doi.org/10.1021/acs.biochem.7b00067, PMID: 28349680

Xiao YS, Schöck F, González-Morales N. 2017. Rapid IFM dissection for visualizing fluorescently tagged sarcomeric proteins. *Bio-Protocol* **7**:e2606. DOI: https://doi.org/10.21769/BioProtoc.2606, PMID: 29423427

Xie Y, Li H, Luo X, Li H, Gao Q, Zhang L, Teng Y, Zhao Q, Zuo Z, Ren J. 2022. IBS 2.0: an upgraded illustrator for the visualization of biological sequences. *Nucleic Acids Research* **50**:W420–W426. DOI: https://doi.org/10.1093/nar/gkac373, PMID: 35580044

Zhou Q, Chu PH, Huang C, Cheng CF, Martone ME, Knoll G, Shelton GD, Evans S, Chen J. 2001. Ablation of Cypher, a PDZ-LIM domain Z-line protein, causes a severe form of congenital myopathy. *The Journal of Cell Biology* **155**:605–612. DOI: https://doi.org/10.1083/jcb.200107092, PMID: 11696561

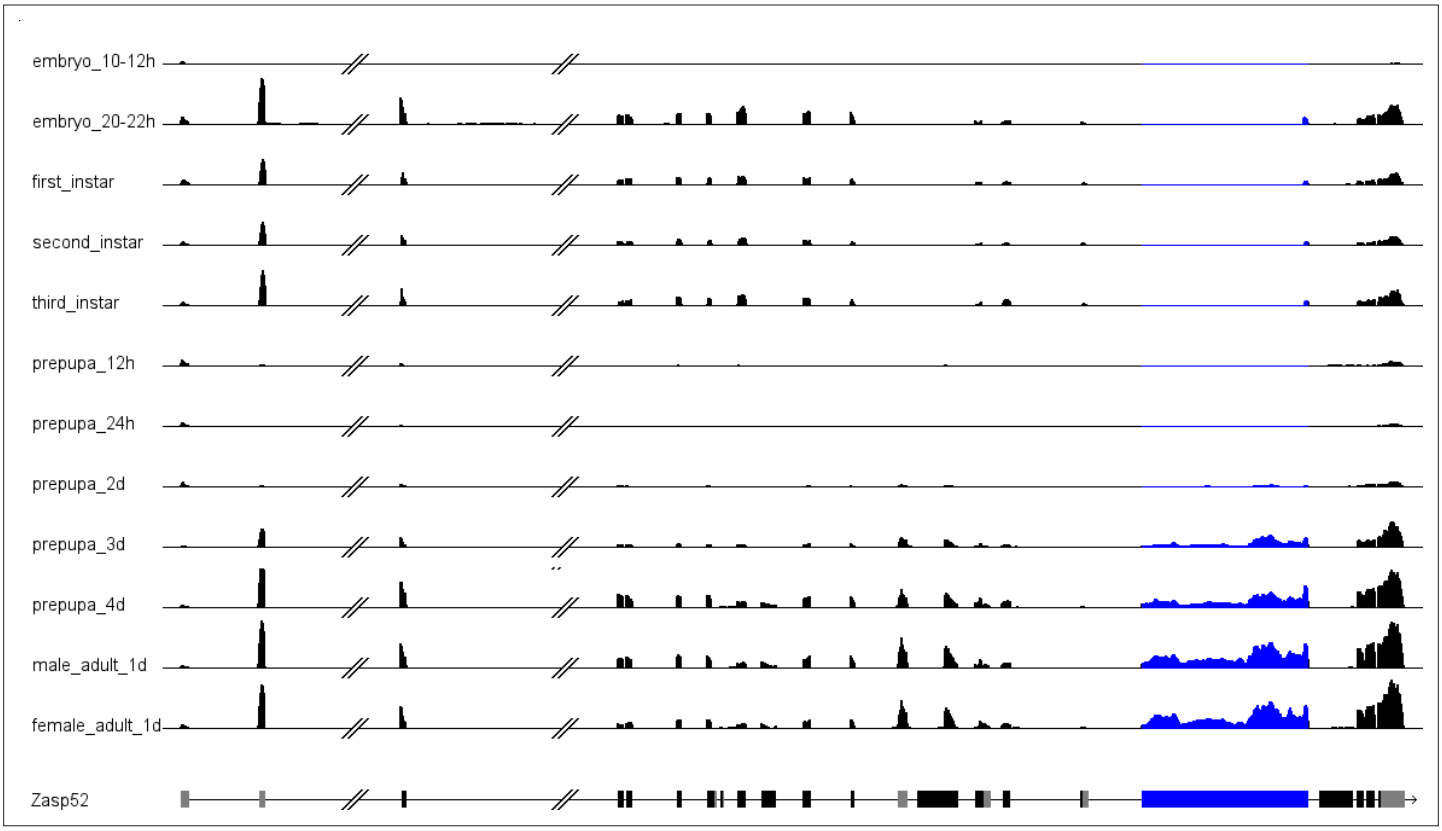

Figure 1—figure supplement 1. RNA-seq data of exon 15e expression. MODENCODE RNA-seq data showing expression levels at the *Zasp52* locus across various developmental stages. Exon 15e is highlighted in blue.

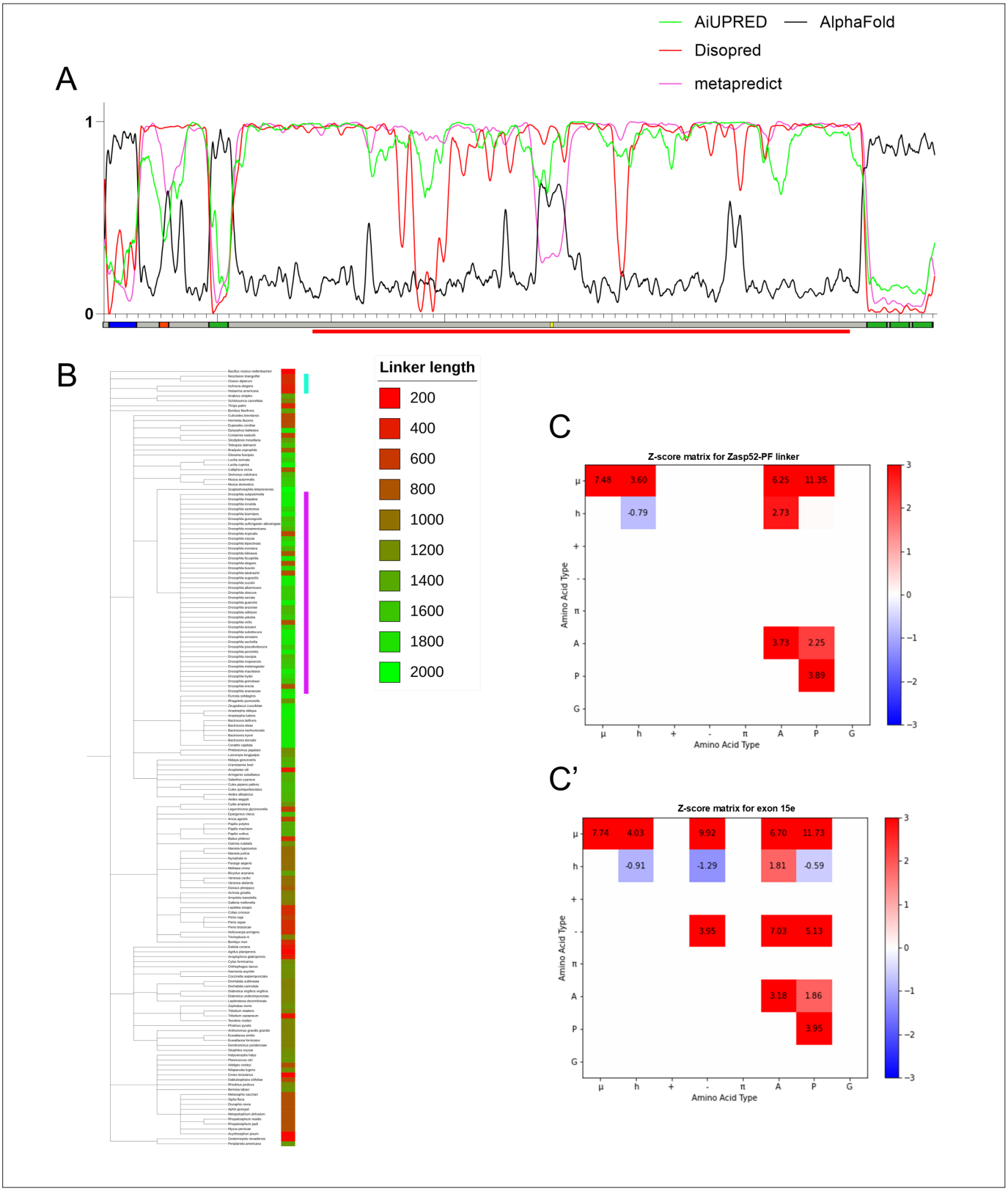

Figure 1—figure supplement 2. Disorder prediction of amino acids encoded by exon 15e. (**A**) Various disorder prediction algorithms were used to assess the level of per-residue disorder at the *Zasp52* locus. The corresponding *Zasp52* locus is schematized below, with PDZ domain (blue), ZM (red), LIM domains (green), and the ABM identified in ***Ashour et al., 2023*** (yellow). The red bar below the Zasp52 schematic indicates the extent of the deletion in *ex15e*. For disorder prediction algorithms (AiUPRED, Disopred, and metapredict), the higher y-values represent higher levels of disorder,

Figure 1—figure supplement 2 continued on next page

Figure 1—figure supplement 2 continued

while low values close to zero represent low levels of disorder (structure). AlphaFold pLDDT scores are plotted alongside in black. pLDDT scores can be used to inform about disorder, with higher scores indicating higher confidence that a region is ordered, and lower scores suggesting disorder (***Ruff and Pappu, 2021***; ***Emenecker et al., 2021***). (**B**) Dendrogram of various insects with Zasp52 orthologs that contain a PDZ domain and four LIM domains. Canonical isoforms, which usually are also the longest ones, were used to compute the number of residues comprising the linker between the first and second LIM domains, with data represented in a heatmap. The purple bar indicates all Drosophilids, and the teal bar indicates species of the order Ephemeroptera and Odonata, which use direct flight. Though some Drosophilids contain shorter linkers, no other species contain linkers of comparable length to Drosophilids and other closely related Dipterans. NARDINI Z-score matrices of the linker region between LIM1 and LIM2 in Zasp52-PF (**C**) and of only the sequence encoded by exon 15e (**C'**). The diagonal squares represent Ω-values, which quantify the linear mixing versus segregation of all of residue type *x* with respect to all other residues. The off-diagonal squares represent δ-values, which quantify the linear mixing versus segregation of pairs of residue types. A high z-score thus indicates segregation/blocking of a certain residue type with respect to itself/others compared to a null model; a low score indicates even dispersion and intermixing. Polar residues μ = {S,T,N,Q,C,H}; hydrophobic residues h = {I,L,V,M}; basic residues + = {R,K}; acidic residues - = {E,D}; aromatic residues π = {F,W,Y}; alanine = A; proline = P; glycine = G.

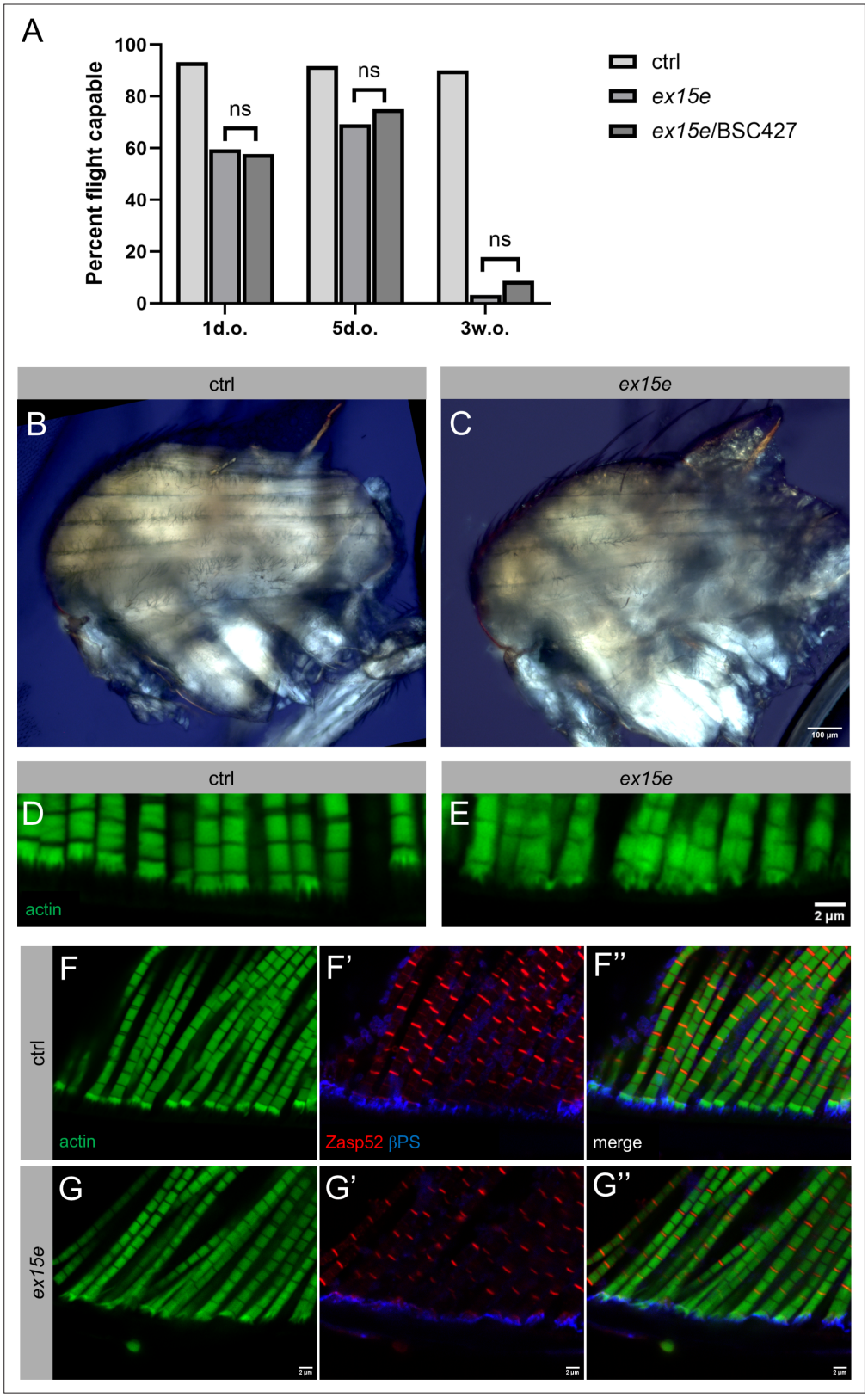

Figure 2—figure supplement 1. Flight assays, gross muscle morphology, and modified terminal Z-discs in *ex15e* mutant. (**A**) A binary flight assay across three age categories of ctrl, homozygous *ex15e*, and *ex15e* over the Zasp52 deficiency *BSC427*. Sample sizes were as follows: 1-day-old (ctrl *n*=44 flies, *ex15e n*=42, *ex15e/BSC427 n*=45), 5-days-old (ctrl *n*=48, *ex15e n*=39, *ex15e/BSC427 n*=28), and 3-weeks-old (ctrl *n*=61, *ex15e n*=30, *ex15e/BSC427*

Figure 2—figure supplement 1 continued on next page

Figure 2—figure supplement 1 continued

n=23). Flight was scored manually on whether they could generate upward lift or not. There was no significant difference between the homozygous mutant or *ex15e* over the deficiency (Fisher's exact test; 1 d.o. p=1.0000; 5 d.o. p=0.7843; 3 w.o. p=0.5729). Polarized light images of sagittally bisected thoraces of 3-week-old ctrl (**B**) and *ex15e* (**C**) revealed no obvious differences in gross morphology; females shown. (**D–G″**) Modified terminal Z-discs (MTZ) were affected in *ex15e*. Close-up views revealed a disruption in the MTZ and adjacent myofibrils in 3-week-old *ex15e* mutants (**E**) compared to ctrl (**D**). The regular 'crown'-shaped structure of the ctrl MTZ is replaced with a disordered structure of variable shape in *ex15e* mutants. βPS integrin and Zasp52 localization appeared unaffected in *ex15e* (**F–G″**). Thin filaments were visualized with phalloidin in green, Z-discs with a Zasp52 full-length antibody in red, and integrin adhesion sites at MTZs with a βPS integrin antibody in blue.